

## CHAPTER 3

# *Quantum Catalysis in Enzymes*

AGNIESZKA DYBALA-DEFRATYKA,<sup>a</sup> PIOTR PANETH<sup>a</sup>  
AND DONALD G. TRUHLAR<sup>b</sup>

<sup>a</sup>Institute of Applied Radiation Chemistry, Technical University of Lodz, Zeromskiego 116, 90-924 Lodz, Poland; <sup>b</sup>Department of Chemistry and Supercomputing Institute, University of Minnesota, 207 Pleasant Street S.E., Minneapolis, MN 55455-0431, USA

### 3.1 Introduction

Enzyme-catalysed reactions span a wide range of reaction types and mechanisms. In many cases the rate-determining step is the transfer of a proton, hydride ion, or hydrogen atom; such reactions are almost always dominated by quantum-mechanical tunnelling. The effective barrier for tunnelling is highly dependent on the evolution of zero-point energy along the reaction path, and zero-point energy is one of the multidimensional effects that one must include in a reliable treatment of quantum-mechanical tunnelling. Even when tunnelling is negligible, changes in the zero-point energy of participating vibrational modes when the system passes from the reactant state to the transition state can have accelerating, or, less often, decelerating effects on reaction rates, and these kinds of vibrational effects, as well as the change in thermal vibrational energy of low-frequency quantised vibrational modes, are very important for studying kinetic isotope effects, which are one of the chief experimental tools for elucidating reaction mechanisms and probing the nature of transition states. Theoretical methods for systematically including the quantum effects of multidimensional tunnelling and quantised vibrations in the description of enzyme-catalysed reactions have been

developed and applied<sup>1–5</sup> and are reviewed from a pedagogical perspective in this chapter.

Aside from quantum-mechanical scattering theory (see Appendix), which is only applicable to very small gas-phase systems, the best available theory of chemical reaction rates is transition-state theory, which has a long history of productive use for chemical reactions in the gas phase, in condensed phases, and in enzymes.<sup>1–14</sup> Transition-state theory in its most basic form is a classical mechanical theory that corresponds to calculating the one-way flux through a coordinate–space hypersurface (usually one just says “surface”) that separates reactants from products.<sup>7,15–17</sup> (More generally, the hypersurface could be defined in phase space, but for enzymatic reactions coordinate space will suffice.) The dividing surface is called the transition state<sup>7,9</sup> (in some of the older literature it was often called the activated complex<sup>8</sup>). The vibrational mode normal to this surface is called the reaction coordinate, although this term is also used to refer to a global progress variable measuring the advance from reactants to the transition state to products. Sometimes, but not always, these two reaction coordinates coincide in the vicinity of the transition state. Note that the transition state is not a single geometric point but rather is the ensemble of all the points in the dividing surface. Transition-state theory employs statistical mechanics to sum the fluxes through all these points (“transition points”), properly weighted for a canonical ensemble.

In a classical-mechanical world, transition-state theory would be exact if the states of the reactant are populated according to a Boltzmann distribution, that is, a canonical ensemble (transition-state theory can also be extended to microcanonical ensembles, but that is more useful for gas-phase reactions than for enzymatic reactions, and it will not be considered further in this chapter), and if no classical trajectories recross the transition state without first being thermalised in the product region of coordinate space (or – for reverse trajectories – in the reactant region of coordinate space). The no-recrossing criterion will be satisfied exactly if the reaction coordinate is separable (that is, if the Hamiltonian may be written as a sum of a term depending only on the reaction coordinate and its conjugate momentum and other terms depending only on the other coordinates and their conjugate momenta, with no cross terms), and it will be approximately valid if the Hamiltonian is approximately separable. (Note that this separability is required not only in the nearby vicinity of the saddle point but also far enough along the reaction coordinate toward reactants and products that trajectories leaving the saddle point in either direction do not reflect back through the dividing surface.)

Quantum-mechanical effects can be incorporated into transition-state theory by two main routes.

In the first route, which has been used since the early days of transition-state theory, quantum effects are incorporated in two steps.<sup>6,8,11,17,19,20</sup> First, all classical-mechanical vibrational partition functions are replaced by partition functions for quantised vibrations<sup>6,8,19</sup> and electronic partition functions are added to account for multiple potential-energy surfaces.<sup>21</sup> The calculated rate constant at this stage is sometimes called hybrid<sup>20</sup> and sometimes called quasiclassical;<sup>14</sup> these labels denote that quantum effects are still not included on the reaction coordinate

at the transition state because that mode of motion is not represented by a partition function. In the second step, one introduces quantum-mechanical effects on the reaction-coordinate motion by multiplying the transition-state theory rate constant by a transmission coefficient. (The multiplicative transmission coefficient is sometimes also used to correct for recrossing.) In the early history of transition-state theory, the tunnelling was usually calculated by a one-dimensional model,<sup>22,23</sup> but it has been known for a long time<sup>24</sup> that (except in special cases where the tunnelling effect is small) one-dimensional treatments are inadequate, and multi-dimensional tunnelling models<sup>20,25–28</sup> must be used. Therefore the transmission coefficient also accounts for some of the effects of the nonseparability of the reaction coordinate. Furthermore, special care must be employed so that the transmission coefficient is normalised consistently with the underlying transition-state calculation.<sup>20,29,30</sup>

In traditional treatments of chemical-reaction dynamics, it is usually assumed that the reaction occurs along a single valley from reactants to products, with this valley centred on a saddle point in the region of the transition state, and this valley is well described in terms of the coordinates of the reagents (that is, the coordinates of solvents and catalysts, if any, are not needed to describe the dividing surface). There are three ways in which this simple form of transition-state theory must be generalised, one of which (A) is important even for simple gas-phase reactions, and the other two of which (B and C) are especially important for enzymes and some other condensed-phase reactions.

(A) When the no-recrossing criterion is satisfied, the transition state may be considered to be a dynamical bottleneck.<sup>17</sup> Sometimes a dynamical bottleneck does exist, but the transition state dividing surface corresponding to this dynamical bottleneck does not pass through the saddle point. In such a case one should not use the conventional definition of a transition state (by which it passes through the saddle point), but rather one should locate the transition state variationally to minimise recrossing.<sup>15,17,18,26,31–34</sup> This is called variational transition-state theory (VTST). In the original formulation of variational transition-state theory, the reaction valley is still centred on, or at least defined by, a single reaction coordinate. Usually this passes through a saddle point, which is called the conventional transition state; however, trial dividing surfaces may be defined at other points along the reaction path, and these are called generalised transition states.

(B) For reactions occurring in the presence of a solvent or catalyst, or in general for condensed-phase reactions, it is convenient to divide the coordinates into two groups, those of the reagents and those of their surroundings. The former may be called solute, substrate, or reagent coordinates (where “reagents” denotes reactants and products), and the latter may be called solvent, bath, or environmental coordinates, with the understanding that the latter include solvent, enzyme, and coenzyme coordinates. We will use the reagent/environment language. It may happen that the description of the best (*i.e.* least recrossed) dividing surface cannot be accomplished entirely in terms of reagent coordinates; that is, one must also include environmental coordinates. Note that describing the dividing surface is equivalent to specifying the reaction coordinate since the latter is normal to the

former. Thus, this effect may be called participation of environmental coordinates in the reaction coordinate. Historically, it has been identified by the confusing label of nonequilibrium solvation. Although this label can be justified, the effect does not involve a breakdown of the Boltzmann distribution, but rather an inability to define a no-recrossed dividing surface unless environmental coordinates are included in the definition of the dividing surface.<sup>35</sup>

(C) Even when the environment is allowed to participate in the reaction coordinate, a liquid-phase or enzymatic reaction may proceed through several different valleys, each going through its own saddle point (multiple passes across a mountain range, arranged as in parallel electric circuits, not in series). In such a case we must consider not just an ensemble of transition points at the mountain pass of one reaction valley (centred on a particular drainage line or valley floor, which may be called a reaction path), but also an ensemble of reaction valleys,<sup>36,37</sup> which may be called an ensemble of reaction paths.

The method of ensemble-averaged variational transition-state theory<sup>2-3,38-40</sup> has been developed to account for features B and C, which can both be very important in enzymatic reactions. At the same time, ensemble-averaged variational transition-state theory is formulated in such a way as to allow the incorporation of quantised vibrations and multidimensional tunnelling contributions. The present chapter surveys this theory with a special emphasis on the quantum effects. A broader review of the incorporation of quantum mechanics into enzyme kinetics modelling is presented elsewhere.<sup>1</sup>

## 3.2 Theory

### 3.2.1 Gas-Phase Variational Transition-State Theory

In conventional transition-state theory (TST) the expression for the thermal rate constant of a bimolecular reaction is given by:

$$k^\ddagger = \frac{k_B T}{h} \frac{Q^\ddagger(T)}{\Phi^R(T)} \exp(-V^\ddagger/k_B T) \quad (3.1)$$

where  $k_B$  is the Boltzmann constant,  $T$  is the temperature,  $Q^\ddagger$  is the vibrationally quantised partition functions of the transition state ( $\ddagger$ ) that, being a surface, is missing one degree of freedom (the reaction coordinate),  $\Phi^R$  is the vibrationally quantised partition function per unit volume of the pair of reactants (R), and  $V$  is the potential energy difference between reactants and the transition state (which is called the classical barrier height). If we set  $V=0$  at the equilibrium state of reactants, then

$$V^\ddagger = V_{\text{MEP}}(s=0) - V_{\text{MEP}}(s=s_R) \quad (3.2)$$

where  $s$  is the reaction coordinate,  $V_{\text{MEP}}(s)$  is the potential energy along the minimum-energy path (MEP) from reactants to products,  $s=0$  denotes the

location of the saddle point (where  $V_{\text{MEP}}$  takes its highest value), and  $s_{\text{R}}$  denotes the reactant value of  $s$  (for a gas-phase bimolecular reaction,  $s_{\text{R}} = -\infty$ ). In formulating eqn (3.1), we removed the coordinates and momenta of the overall centre of mass, which is irrelevant. Thus,  $Q^{\ddagger}(T)$  has no translational partition function, but  $\Phi^{\text{R}}$  has a relative translational partition function, which is why it is included on a per volume basis. Note that for a liquid-phase reaction the relative translational degree of freedom is better considered to be a relative liberational<sup>41</sup> coordinate. The transition-state-theory approximation can be improved by introducing a transmission coefficient that can be further divided into three contributions:

$$k = \Gamma(T)g(T)\kappa(T)k^{\ddagger}(T) \quad (3.3)$$

In this equation  $\Gamma$  describes deviation from the no-recrossing assumption; it can often be neglected if there is a single reaction path and the location of the dynamical bottleneck is variationally optimised along this path. The factor  $g$  is a measure of the deviation from the assumption<sup>42</sup> that reactant molecules are locally equilibrated, and  $\kappa$  introduces the contribution from the nonclassical transmission through the barrier and is usually dominated by tunnelling but also includes nonclassical reflections. By the very nature of recrossing,  $\Gamma$  accounts for nonseparability of the reaction coordinate, but, as mentioned above, multi-dimensional tunnelling models, used for  $\kappa$ , also account for reaction-coordinate nonseparability.

For reactions in which energy transfer is fast enough to keep the relative population of the reactant states at equilibrium,  $g$  is approximately equal to unity,<sup>4,43–46</sup> and only the remaining two factors of the transmission coefficient need to be considered. Instead of including  $\Gamma(T)$  to correct eqn (3.1), we can employ VTST, where  $k^{\ddagger}(T)$  is replaced by a variational transition-state theory rate constant so that  $\Gamma(T)$  is usually small enough to be neglected. Thus, one replaces eqn (3.3) by a combination of a transmission coefficient  $\kappa$  and VTST, where  $\kappa$  accounts for quantum effects on the reaction coordinate. We shall, however, reintroduce  $\Gamma$  when we consider ensemble-averaged VTST.

We will discuss the inclusion of quantum effects in canonical VTST, that is, VTST for a canonical ensemble; this is usually called canonical variational theory (CVT). In CVT<sup>33,34</sup> the transition state is optimised with respect to  $s$ , a distance, along a given reaction path, most frequently the minimum-energy path (MEP), from the saddle point, which location by convention is at  $s=0$ . The optimisation consists of varying the location of the dividing surface (generalised transition state) by placing it so that the forward flux through it is minimised.<sup>15,31–34,47–49</sup>

The expression for the rate constant analogous to that given by eqn (3.1) is:

$$k^{\text{CVT}} = \kappa(T) \frac{k_{\text{B}}T}{h} \frac{Q^{\text{GT}}(T, s_{*}^{\text{CVT}}(T))}{\Phi^{\text{R}}(T)} \exp(-V_{\text{MEP}}(s_{*}^{\text{CVT}}(T))/k_{\text{B}}T) \quad (3.4)$$

where  $\Phi^R$  is the quantised partition function per unit volume of the reactant,  $Q^{GT}$  is the quantised partition function of the generalised transition state at location  $s$  along the reaction path, and  $s^{CVT}$  is the location of the CVT dividing surface. The variational dividing surface is labelled with “\*” to clearly distinguish it from the conventional TST one at  $s=0$  that is labelled with “‡”. The quasithermodynamic equivalent to eqn (3.4) is:

$$k^{CVT} = \kappa(T) \frac{k_B T}{h} K^{\ddagger,0} \exp\left(-\Delta G_T^{CVT,0} / RT\right) \quad (3.5)$$

where  $K^{\ddagger,0}$  is the reciprocal of concentration in the standard state for bimolecular reactions,  $R$  is the universal gas constant, and

$$\Delta G_T^{CVT,0} = \max_s \Delta G_T^{GT,0}(s) \quad (3.6)$$

where  $\Delta G_T^{GT,0}$  is the generalised<sup>50</sup> standard-state free energy of activation<sup>8–9,51–53</sup> for the trial dividing surface at  $s$  at temperature  $T$ . Equation (3.5) is called quasithermodynamic because the generalised transition states are missing one degree of freedom (and thus are not true thermodynamic species), and  $\Delta G_T^{GT,0}$  is called generalised because we do not restrict the transition state to pass through the saddle point as in conventional TST.

When there are two or more local maxima in  $\Delta G_T^{GT,0}$  in series as a function of  $s$ , one may account for them by the canonical unified statistical (CUS) model,<sup>54,55</sup> which is an extension of the microcanonical unified statistical (US) model.<sup>56,57</sup> In these models, one recognises that a system can be thermalised or randomised as an intermediate between dynamical bottlenecks. In the limit when the intermediate corresponds to a deep well, the system may exit with equal likelihood in either direction. This can introduce a transmission coefficient between 0.5 and 1.

Equations (3.1)–(3.6) can also be extended to unimolecular reactions in solution, which is a good starting point for treating the catalytic step in most enzyme reaction since this step is usually the reaction of a Michaelis complex. To do this generalisation, one replaces  $\Phi^R$ , which is a partition function per unit volume, by  $Q^R(T)$ , which is a unitless partition function, since there is no translation (and hence no volume factor to remove), one sets  $s^R$  to a finite negative value, and one includes solvent effects on  $V_{MEP}$ , on the partition coefficients, and on the transmission coefficient  $\kappa$ .

When the solvent does not participate in the reaction coordinate and when the temperature dependence of the free energy of solvation may be neglected in calculating the effective potential for tunnelling, solvent effects may be included in  $\kappa$  by replacing the potential energy of the solute by its potential of mean force as a function of all solute coordinates.<sup>30,58</sup>

If desired, one can optimise the shape and orientation of the dividing surface as well as the location at which it intersects the MEP.<sup>59–61</sup> In fact it is strongly recommended to define the reaction coordinate (and hence the dividing surface, which is the hypersurface corresponding to some constant value of the reaction

coordinate) in curvilinear coordinates;<sup>60</sup> this corresponds to a curved dividing surface (as opposed to the hyperplane defined by a Cartesian treatment).

CVT accounts for the recrossing of the conventional transition state by choosing a better location for the transition state. CVT includes quantum effects on degrees of freedom orthogonal to the reaction by quantising partition functions, just as in conventional TST. Even more important in many cases, though, is that VTST allows a consistent treatment of the nonclassical penetration of the reaction barrier, *i.e.* quantum effects on the reaction coordinate. The most important part of the theoretical evaluation of the rate constants for many reactions is estimation of the tunnelling contributions. There are two aspects to this inclusion. One is the tunnelling dimensionality and the other its directionality. Before going into the details of tunnelling we will briefly discuss these two issues and categorise basic “types” of tunnelling.

### 3.2.2 The Transmission Coefficient

Inclusion of tunnelling requires substantially more information about the energetic landscape of the reaction than is necessary to describe the same reaction without including  $\kappa$ . In consequence, the calculations are more time consuming.

The quantum-mechanical probability of tunnelling depends on the energy of the reactants, the masses of the atoms that move during the process (actually, they all move, but light atoms participating strongly in the reaction coordinate or strongly coupled to it move in the most significant ways, and it is their masses that matter the most), the width and shape of the effective barrier, and the nature of the tunnelling paths. The dependence of the tunnelling probability on the barrier shape and tunnelling paths is the main reason for the already mentioned extra cost of the quantum-mechanical calculations of rate constants because the shape of the potential energy or potential of mean force landscape cannot be restricted to the vicinity of stationary points when calculating the tunnelling probability.

As stated in Section 3.1, early models treated the tunnelling problem as a one-dimensional problem, in particular, they modelled tunnelling based only on the probability of transmitting a mass point through a one-dimensional analytic<sup>23,62</sup> barrier. Technically, these calculations were quite simple, and they required a minimum of information about the potential-energy surface. This approximation not only neglects contributions from other coordinates but also from cross terms and couplings. Sometimes these methods strongly underestimate the tunnelling contribution to the total reaction flux, but they can also provide overestimates.

Calculations of tunnelling contributions based on considering more than one coordinate are called multidimensional models. The simplest one is called zero-curvature tunnelling (ZCT), and it differs from the one-dimensional models in that quantisation of all vibrational modes along the MEP is included. Since the vibrational frequencies change along the reaction paths, so do the quantised energy requirements. If vibrations orthogonal to the reaction coordinate retain their state (*i.e.* retain their quantum numbers, *i.e.* evolve vibrationally adiabatically), their energy must be added to the potential energy. Whereas  $V_{\text{MEP}}$

ultimately (by the Born–Oppenheimer approximation<sup>63–66</sup>) represents the energy tied up in electronic energy and nuclear repulsion because the electronic state evolves adiabatically (*i.e.* does not change) in a thermal reaction, the difference between the vibrationally adiabatic ground-state potential-energy curve and  $V_{\text{MEP}}$  represents the quantised vibrational energy of modes transverse to the reaction coordinate that is also tied up and is unavailable for reaction–coordinate motion if the system is locally vibrationally adiabatic<sup>29,67–77</sup> all along the reaction path. When all vibrations are in their ground (G) state they produce the following effective potential:<sup>29,69,70,77</sup>

$$V_{\text{a}}^{\text{G}} = V_{\text{MEP}}(s) + \epsilon_{\text{vib}}^{\text{G}}(s) \quad (3.7)$$

where “a” stands for adiabatic, and  $\epsilon_{\text{vib}}^{\text{G}}$  is the local zero point vibrational energy;  $V_{\text{a}}^{\text{G}}$  is called the vibrationally adiabatic ground-state potential curve. Often it is more convenient to work with the relative vibrationally adiabatic ground-state potential-energy curve defined by

$$\Delta V_{\text{a}}^{\text{G}} = V_{\text{a}}^{\text{G}}(s) - V_{\text{a}}^{\text{G}}(s = s^{\text{R}}) \quad (3.8)$$

The justification for considering that  $V_{\text{a}}^{\text{G}}$  or  $\Delta V_{\text{a}}^{\text{G}}$  provides an effective barrier for tunnelling is presented elsewhere.<sup>18,20,25,29,67–77</sup> ZCT can be considered an intermediate approximation between one-dimensional models and the full multidimensional models described below.

The models described above differ in dimensionality but as a common feature have tunnelling paths being identical with the MEP. Although the wavefunctions decay most slowly when the system tunnels under the lowest-energy part of the lowest barrier, the distance over which this decay operates depends on the tunnelling path. Thus, the optimum path is a compromise between the path length and the effective potential along the path. As a result, the optimum tunnelling path does not coincide with the MEP but occurs on its concave site. Effectively, the tunnelling path is thus shorter than MEP.<sup>17,19,25,74,78–88</sup> This is called the “corner-cutting” effect, and it will be discussed more fully in Section 3.2.2.2.

In order to calculate the multiplicative transmission coefficient  $\kappa$  one should optimise the tunnelling path, *e.g.*, find a path that minimises semiclassical imaginary action integrals, which in turn maximise the tunnelling probability.<sup>84,89–91</sup> This path is called the least-action path (LAP). The costly effort of searching for the LAP is not usually required. Instead, it is usually sufficient to employ an approximate variational procedure called optimised multidimensional tunnelling<sup>27,28,92,93</sup> (OMT). This method is based on two approximations, one called small-curvature tunnelling<sup>94,95</sup> (SCT) and the other called large-curvature tunnelling<sup>82,92–94,96,97</sup> (LCT), which assume that the curvature of the reaction path is small and large, respectively. The SCT is accurate for small-to-intermediate curvature, while LCT is accurate for intermediate-to-large curvature. The SCT approximation extends the physical model that underlies the Marcus and Coltrin

approximation for the collinear  $\text{H} + \text{H}_2$  identity reaction<sup>25</sup> to general three-dimensional polyatomic reactions; the effective potential is vibrationally adiabatic. The LCT approximation involves tunnelling with a partly vibrationally adiabatic and partly vibrational nonadiabatic potential along a weighted set of straight-line paths. Both approximations will be discussed in Section 3.2.2.2. The SCT and LCT tunnelling probabilities ( $P$ ) are evaluated for each tunnelling energy  $E$ , and the larger tunnelling probability is selected, yielding the so-called microcanonically optimised multidimensional tunnelling ( $\mu\text{OMT}$ ) approximation, also called OMT for short:

$$P^{\mu\text{OMT}} = \max \left\{ \begin{array}{l} P^{\text{SCT}}(E) \\ P^{\text{LCT}}(E) \end{array} \right. \quad (3.9)$$

Making the assumption<sup>18,29</sup> that the vibrationally adiabatic potentials of all excited vibrational states that contribute appreciably to the thermally averaged rate have the same shape as the ground-state one, the transmission coefficient is given by:

$$\kappa = \frac{1}{k_{\text{B}}T} \frac{\int_0^{\infty} dE \exp(-E/k_{\text{B}}T) P^{\text{G}}(E)}{\exp[-V_{\text{a}}^{\text{G}}(s = s_*^{\text{CVT}})/k_{\text{B}}T]} \quad (3.10)$$

where  $V_{\text{a}}^{\text{G}}$  is the ground-state vibrationally adiabatic potential curve described by eqn (3.7), and  $P^{\text{G}}(E)$  is the ground-state quantum-mechanical transmission probability at energy  $E$ . The numerator of eqn (3.10) is proportional to the thermal average of the  $\mu\text{OMT}$  ground-state transmission probability, and the denominator is proportional to the thermal average of the ground-state transmission probability implied by CVT when used without a transmission coefficient. The latter probability corresponds to classical motion along the reaction coordinate and equals a step function at  $E$  equal to  $V_{\text{a}}^{\text{G}}(s = s_*^{\text{CVT}})$ , where  $s_*^{\text{CVT}}$  is defined below eqn (3.4). By detailed balance, the exact transmission coefficient is the same for the forward and reverse reactions, so one needs to calculate only one of them; for non-thermoneutral reactions, the convention used in the LCT approximation is to always calculate  $P^{\text{G}}$  in the exoergic direction. The G in  $P^{\text{G}}$  refers to the ground state of reactants. Since the SCT approximation is vibrationally adiabatic, tunnelling proceeds only into the ground vibrational state of products. However, although the theory is vibrationally adiabatic in the tunnelling region, it does not require the system to be vibrationally adiabatic either before or after that region, and most reactants are *not* vibrationally adiabatic for low-frequency vibrations or rotations in the reactant and product regions. The LCT approximation is not vibrationally adiabatic even in the tunnelling region, and the tunnelling probability is summed over final states.

The generalisation of these procedures to reactions governed by liquid-phase potentials of mean force (PMFs, which are free energies) rather than gas-phase potential energies is given elsewhere.<sup>30,58,98,99</sup>

“Tunnelling” is actually a correct description of the quantum-mechanical reaction–coordinate motion only for energies below the vibrationally adiabatic barrier height. Above that, the classical transmission probability would be equal to unity, but the quantal one only gradually approaches unity as the energy is increased still further (this will be illustrated in Section 3.3.4). The deviation from unity is called nonclassical reflection; it may be envisioned as diffraction of the deBroglie wave by the barrier top. Although nonclassical reflection for an energy  $\Delta E$  above the effective barrier top is comparable in magnitude to tunnelling for an energy  $\Delta E$  below the effective barrier top,<sup>68,100–102</sup> the energies at which nonclassical reflection occurs are weighted by smaller Boltzmann factors than those for energies below the barrier tops, where tunnelling occurs; thus nonclassical reflection has only a small effect on most rate constants. In the OMT approximation it is treated by a parabolic uniformisation procedure.<sup>100–102</sup>

We have described how the various elements of a multidimensional tunnelling calculation are put together, and what remains is to describe how the tunnelling probability itself,  $P^G$ , is calculated. We present that next in two stages: first (Section 3.2.2.1) a pedagogical introduction to quantum-mechanical tunnelling theory, and second (Section 3.2.2.2) a brief overview of how this is extended to multidimensional tunnelling.

### 3.2.2.1 One-Dimensional Tunnelling

We begin with a quantum-mechanical description of the one-dimensional motion of a particle of mass  $m$  governed by a potential-energy function  $V$ . The local kinetic energy is

$$T = E - V(x) \quad (3.11)$$

where  $E$  is the total energy. The local momentum is

$$p = \sqrt{2m[E - V(x)]} \quad (3.12)$$

If  $V$  were constant,  $p$  would also be constant, and the wavefunction would be

$$\psi = e^{ipx/\hbar} \quad (3.13)$$

Next we introduce the Wentzel–Kramers–Brillouin (WKB) approximation,<sup>100–103</sup> a “semiclassical” approximation in which the wavefunction is approximated, to lowest order in  $\hbar$ , by

$$\psi \sim e^{i \int^x p(x') dx' / \hbar} \quad (3.14)$$

Since the word “semiclassical” is used with a myriad of meanings (*e.g.*, some workers use it to denote what we here call “quasiclassical,” other workers use it

for treatments of a multidimensional system in which some coordinates are classical and others are quantal, *etc.*), we emphasise that the word “semi-classical” refers here to expanding of the phase of the wavefunction in powers of  $\hbar$  and truncating the expansion to yield an approximate wavefunction part way between quantum mechanics and classical mechanics.<sup>103</sup>

There are two noteworthy aspects of eqn (3.14). First, it replaces the solution of a differential equation by a quadrature. Second, as emphasised by Smith,<sup>104</sup> this expression involves computing an approximate wavefunction by integrating over the coordinate and momentum variables of an actual classical motion, and the resulting integral in eqn (3.14) is the classical action of the one-dimensional classical trajectory.

When, at some location  $x$ ,  $V > E$ , the kinetic energy is negative at that  $x$ , and the classical momentum is imaginary; the approximation to the wavefunction becomes

$$\psi \sim e^{-\int^x |p(x')| dx' / \hbar} \quad (3.15)$$

The primitive approximation to the tunnelling amplitude becomes<sup>103</sup>

$$T_{\text{tun}} = e^{-\theta(E)/\hbar} \quad (3.16)$$

$$\theta = \int_{\xi_{\text{R}}}^{\xi_{\text{P}}} |p(\xi)| d\xi \quad (3.17)$$

where  $\theta$  is the magnitude of the imaginary part of the action integral over the tunnelling region of  $x$ ,  $\xi_{\text{R}}$  is the beginning of the tunnelling region (where  $E = V(x_{\text{R}})$ ) on the reactant side, and  $\xi_{\text{P}}$  is where the particle emerges from under the barrier on the product side (where  $E = V(x_{\text{P}})$ ). Note that  $\xi$  is a progress variable along the tunnelling path; it is a dummy variable, and it could equally well be called  $x$  or  $x'$ . The tunnelling probability is the absolute square of the tunnelling amplitude:

$$P = e^{-2\theta/\hbar} \quad (3.18)$$

When  $x_{\text{R}}$  is close to  $x_{\text{P}}$ , this approximation breaks down. When  $E$  equals the maximum value of  $V$ ,  $x_{\text{R}}$  becomes the same as  $x_{\text{P}}$ , and the primitive approximation to  $P$  in eqn (3.18) tends to unity. The correct result is of the order of one half, and for a parabolic barrier it is exactly one half.<sup>100,103</sup> This is corrected by the parabolic uniformisation<sup>100–102</sup> mentioned above, which yields

$$P = \frac{1}{1 + e^{2\theta/\hbar}} \quad (3.19)$$

When  $P$  is small (“deep tunnelling”), eqns (3.18) and (3.19) agree well. We always use the latter.

### 3.2.2.2 Multidimensional Tunnelling

For a one-dimensional problem there is only one path through the barrier, namely along  $x$  from  $x_R$  to  $x_P$ . For a multidimensional problem there is a choice of paths. To extend eqn (3.19) to a multidimensional case we must specify the tunnelling path or paths, prescribe how to average over the paths if there is more than one path to be considered at a given  $E$ , and provide a prescription for  $\xi$ ,  $\xi_R$ ,  $\xi_P$ , and  $p(\xi)$  in eqn (3.17). In general we write

$$p = \sqrt{2\mu_{\text{eff}}(\xi)[E - V_{\text{eff}}(\xi)]} \quad (3.20)$$

where  $\mu_{\text{eff}}$  and  $V_{\text{eff}}$  are, respectively, the effective reduced mass and the effective potential along a given tunnelling path.

In a general coordinate system, the reduced mass depends on the direction of motion. Consider, for example, the collision of an atom A with a diatomic molecule BC. There are nine coordinates, which may be written as the components of a 9-vector

$$\mathbf{q} = \begin{pmatrix} R_{BC,x} \\ R_{BC,y} \\ R_{BC,z} \\ R_{A,BC,x} \\ R_{A,BC,y} \\ R_{A,BC,z} \\ R_{ABC,x} \\ R_{ABC,y} \\ R_{ABC,z} \end{pmatrix} \quad (3.21)$$

where  $\mathbf{R}_{BC}$  is a 3-vector from B to C,  $\mathbf{R}_{A,BC}$  is a 3-vector from A to the centre of mass of BC, and  $\mathbf{R}_{ABC}$  is a 3-vector from the origin to the centre of mass of ABC. Motion in the direction of any of the components of  $\mathbf{R}_{BC}$  has a reduced mass equal to  $m_B m_C / (m_B + m_C)$ , motion in the direction of the components of  $\mathbf{R}_{A,BC}$  has the reduced mass of  $(m_A m_{BC} / m_A + m_{BC})$ , and motion along any of the three component directions of  $\mathbf{R}_{ABC}$  has the reduced mass  $m_{ABC}$ , which is the total mass of the system. The coordinate system of eqn (3.21) is usually called the Jacobi coordinate system because of its historical use by Carl Jacobi to treat 3-body problems in planetary mechanics. We could equally well have used the atomic Cartesians,  $\mathbf{R}_A$ ,  $\mathbf{R}_B$ , and  $\mathbf{R}_C$ , with reduced mass  $m_A$ ,  $m_B$ , and  $m_C$ , respectively. Notice that the Jacobi coordinates are linear combinations of atomic Cartesians, *e.g.*

$$R_{A,BC,y} = R_{A,y} - \frac{m_B R_{B,y} + m_C R_{C,y}}{m_B + m_C} \quad (3.22)$$

Any coordinates that are linear combinations of atomic Cartesian coordinates are called rectilinear coordinates because a straight line in atomic

Cartesian transforms into a straight line in any such coordinate system. It is straightforward to find the reduced mass for any straight motion in a rectilinear coordinate system, and such a reduced mass is a constant, as in the examples above.

As mentioned above, between eqns (3.8) and (3.9), the optimum tunnelling path is the least-action path that, for tunnelling, is a shorthand way of referring to the path with least imaginary action. This is a generalisation of a least-action principle of classical mechanics,<sup>105–108</sup> but now it is applied to a trajectory with complex momenta (for the one-dimensional problem above, the momentum was purely imaginary, but for multidimensional problems it could be real or almost real in some directions, for example, those corresponding to spectator coordinates, and imaginary or complex in other directions). In order to find the least-action tunnelling path one needs to know  $\mu_{\text{eff}}$  and  $V_{\text{eff}}$  for motions along arbitrary paths.

One way to simplify this problem is to transform to isoinertial coordinates. Isoinertial coordinates are rectilinear coordinates in which the reduced mass is the same for straight-line motion in all directions. Vibrational spectroscopists usually use mass-weighted Cartesian coordinates<sup>109,110</sup> in which each atomic Cartesian  $R_{A,\alpha}$  (with  $\alpha = x, y, \text{ or } z$ ) is transformed to

$$q_{A,\alpha} \equiv \sqrt{m_A} R_{A,\alpha} \quad (3.23)$$

where  $q_{A,\alpha}$  is a generalised coordinate. This transforms the kinetic energy from

$$T = \frac{1}{2} \sum_A \sum_{\alpha} m_A \dot{R}_{A,\alpha}^2 \quad (3.24)$$

where an overdot denotes a time derivative, to

$$T = \frac{1}{2} \sum_A \sum_{\alpha} \dot{q}_{A,\alpha}^2 \quad (3.25)$$

Equation (3.25) shows that mass-weighted coordinates are isoinertial with a unitless mass of unity and with coordinates that have units of  $(\text{mass})^{1/2}$  (distance). Such units are inconvenient, confusing, or both, so we prefer mass-scaled generalised coordinates defined by

$$Q_{A,\alpha} = \sqrt{\frac{m_A}{\mu}} R_{A,\alpha} \quad (3.26)$$

which convert the kinetic energy to

$$T = \frac{1}{2} \mu \sum_A \sum_{\alpha} \dot{Q}_{A,\alpha}^2 \quad (3.27)$$

where  $\mu$  is an arbitrary mass, which is usually taken as 1 amu (in older papers on gas-phase bimolecular reactions we typically took it as the reduced mass of relative translation of reactants, for example,  $\mu_{A,BC}$  for an atom–diatom collision of A with BC). Note that one can also obtain an isoinertial coordinate system with reduced mass  $\mu$  by starting with Jacobi coordinates and scaling them by  $(\mu_{AB}/\mu)^{1/2}$ ,  $(\mu_{A,BC}/\mu)^{1/2}$ , and  $(\mu_{ABC}/\mu)^{1/2}$ , respectively. In fact there are an infinite number of isoinertial coordinate systems, but they are all related by orthogonal transformations; thus, *e.g.*, the MEP is the same in all of them.<sup>19</sup> In isoinertial coordinates, the motion of  $N$  particles in 3 dimensions becomes equivalent to the motion of a single particle in  $3N$  dimensions.<sup>105a</sup> Furthermore, straight-line paths in atomic Cartesian coordinates transform into straight-line paths in isoinertial coordinates; thus isoinertial cases are a special case of “rectilinear”<sup>110a</sup> coordinates.

Minimisation of the tunnelling action integral of eqns (3.17) and (3.20) can be accomplished by choosing the path with the optimum combination of small effective reduced mass (because the square root of the effective mass appears in the integrand; see eqns (3.17) and (3.20)), short length (because the action integral is an integral over the length of the path), and low barrier (because  $[V_{\text{eff}}(x) - E]^{1/2}$  appears in the integrand). This is simpler in isoinertial coordinates because all directions have the same reduced mass, so the compromise of three factors reduces to a compromise of two, namely path length and barrier. In general, the tunnelling path is shortened by corner cutting, that is, the tunnelling path is on the concave side of the MEP; this increases the barrier as compared to tunnelling along the MEP, and the best compromise is determined by eqns (3.17), (3.19), and (3.20).

Although it has been known for a long time that it is inaccurate to take the tunnelling path as the MEP,<sup>24,111</sup> tunnelling along the MEP provides a good starting point for discussion and a good reference for measuring the extent of corner cutting. Taking the tunnelling path as the MEP is called the zero-curvature tunnelling approximation because if the MEP were straight (had zero curvature) in isoinertial coordinates, the MEP would indeed be the most favourable tunnelling path. In the ZCT approximation,  $\xi$  is simply the distance  $s$  along the MEP,  $\mu_{\text{eff}}$  is  $\mu$  (the scaling mass of the isoinertial coordinate system being used), and  $V_{\text{eff}}$  is as defined in eqn (3.7). There are three reasons for using the  $V_{\text{a}}^{\text{G}}$  of eqn (3.7) rather than  $V_{\text{MEP}}$  as the effective potential for tunnelling. First, it is the only choice consistent<sup>29,69</sup> with transition-state theory, which assumes<sup>6</sup> quantised vibrational modes at the transition state. Second, extensive empirical evidence has accumulated that energy requirements of quantised vibrations are consistent with experimental data on kinetic isotope effects.<sup>112</sup> Third, accurate quantum-mechanical scattering calculations show that quantised vibrational energy requirement quantitatively predict threshold energies for overbarrier reaction.<sup>68,72,75,76,111,113</sup>

When reaction-path curvature is small, one may make the following argument. In the limit of small curvature, the only corner cutting that is advantageous is that which has no energetic penalty. Since the system has zero-point energy in modes transverse to the reaction path, any path between the zero-point

vibrational turning points of the transverse modes should incur no additional energy requirement. A path satisfying this criterion that is dynamically favourable when internal centrifugal effects are dominant is a smooth path that rides close to the envelope of vibrational turning points on the concave side of the MEP in the direction of the reaction-path curvature. The distance along this path must be modelled in a way that does not fail when the distance from the MEP to the turning point exceeds the radius of curvature. Putting these elements together yields the small-curvature tunnelling (SCT) approximation.

A key element in the SCT approximation is that the tunnelling is calculated for a single dominant tunnelling path at each tunnelling energy. In the small-curvature regime, this is a much better model of the tunnelling process than averaging over tunnelling paths.<sup>74</sup>

In the limit where reaction-path curvature is large, straight-line tunnelling paths provide the best approximation because the amount of path shortening that can be accomplished in isoinertial coordinates by corner cutting becomes very large.<sup>82-85</sup> In this limit it is sometimes competitive to tunnel even before reaching the point where  $V_a^G(s)=E$ . Thus, several tunnelling paths contribute even at a given tunnelling energy and even for tunnelling into a given final state. Furthermore, in the LCT approximation one must consider tunnelling directly into excited vibrational states (sometimes this even dominates the rate).<sup>85,114</sup> Figure 3.1 illustrates the general characters of typical tunnelling paths in the LCT approximation. Although the reaction is not dominated by as narrow a distribution of tunnelling paths as those that dominate in the small-curvature

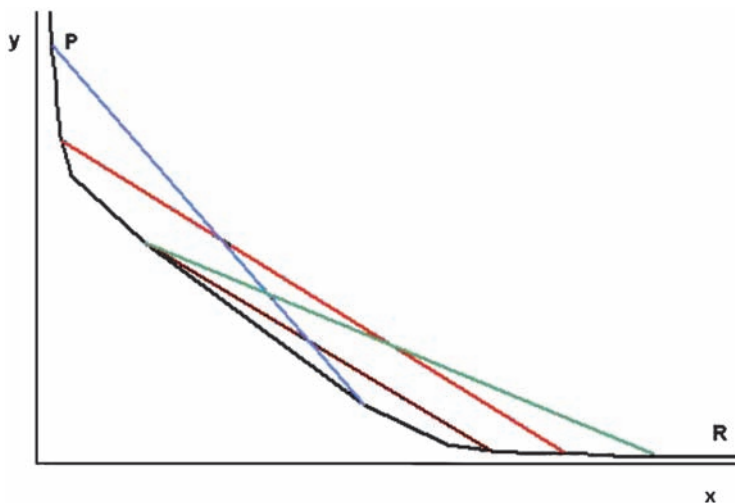


**Figure 3.1** Schematic illustration of LCT tunnelling paths; R and P denote reactant and product regions, the black curve from R to P is an MEP, and the abscissa and ordinate are the bond lengths of the forming and breaking bonds. The blue, green, and red curves are schematic representations of possible LCT tunnelling paths for various systems.

case, one can still identify representative tunnelling paths and draw certain generalisations, for example, that deuterium typically tunnels at a smaller donor–acceptor distance than protium.<sup>85</sup> One can also make analogies to electron-transfer theory, *e.g.*, the straight line paths may be visualised as analogues of a sudden or Franck–Condon transition.<sup>51</sup>

Full details of the procedures for carrying out CVT overbarrier calculations and ZCT, SCT, LCT, and OMT tunnelling calculations are given elsewhere.<sup>28,55,94,97</sup> These tunnelling approximations are collectively referred to as examples of multidimensional tunnelling (MT), and the use of CVT with any of them is called VTST/MT or CVT/MT.

### 3.2.3 Ensemble Averaging

As mentioned above, VTST can be extended to reactions in condensed phases. When a liquid-phase reaction is not in the diffusion-controlled limit, the bimolecular rate constant can be written as:

$$k^{\text{CVT}} = \kappa(T) \frac{k_{\text{B}}T}{\hbar C^{\circ}} \exp\left\{-[G_T^{\circ}(\text{CVT}) - G_T^{\circ}(\text{R})]/RT\right\} \quad (3.28)$$

where  $C^{\circ}$  is the concentration corresponding to the standard state,  $G_T^{\circ}(\text{R})$  is the condensed-phase standard-state free energy of reactants at temperature  $T$ , and  $G_T^{\circ}(\text{CVT}) - G_T^{\circ}(\text{R})$  is the condensed-phase standard-state free energy of activation<sup>8,9,50–53</sup> at temperature  $T$ . Analogously to the gas-phase case, the variational free energy of activation is given by:

$$\Delta G_T^{\circ} = \max_s \Delta G_T^{\circ}(\text{GT}, s) \quad (3.29)$$

where  $\Delta G_T^{\circ}(\text{GT}, s)$  is the standard-state free energy of activation for a generalised transition state at a location  $s$  along the reaction path.

In condensed-phase reactions the generalised-transition-state dividing surface may depend on more than just the solute coordinates. It can, for example, depend on the protein coordinates for an enzyme-catalysed reaction. While for a simple reaction in the gas phase almost all of the reaction flux passes through a single TS on a single reaction path, an enzyme-catalysed reaction may proceed through a large number of reaction paths, each passing through a different saddle point. In fact, the number of saddle points may be so numerous that they must be treated by statistical-mechanical theories. One way to account for this situation is to sample the space of saddle points and average the results – this can be accomplished by ensemble-averaged<sup>2,3,38–40</sup> VTST (EA-VTST). It can be augmented by the inclusion of the tunnelling contributions in the same way as discussed for the gas-phase reactions; this results in the EA-VTST/OMT<sup>2,3,38–40</sup> method. Sometimes it is not necessary to optimise the tunnelling paths. EA-VTST with any of the multidimensional tunnelling approximations (ZCT, SCT, LCT, or OMT) is called simply EA-VTST/MT.

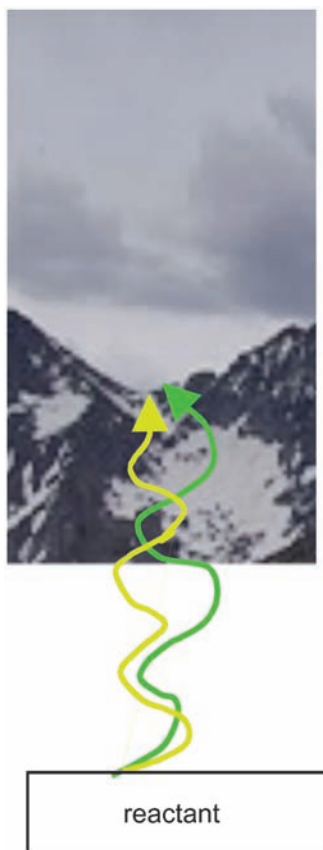


**Figure 3.2** In the gas phase or a crystal, transition-state theory accounts for all trajectories in a valley through a dividing surface at or near the saddle point.

Figure 3.2 illustrates that a VTST calculation based on a single reaction path samples an ensemble of trajectories or wave packets associated with that path. Figure 3.3 illustrates that EA-VTST samples several parallel reaction paths. Each reaction path is the MEP for a primary reaction zone (*e.g.*, the substrate and key parts of the enzyme, coenzyme, or solvent) with the rest of the system (called the secondary reaction zone) temporarily approximated as frozen. Since the reaction paths are different for different secondary reaction zone configurations, this allows the secondary reaction zone to participate in the reaction coordinate, in the language introduced in Section 3.1 (see items B and C in that section). Because the transmission coefficient for individual reaction paths does not include the motion of the secondary reaction zone as a function of progress along the reaction coordinate, this is called the static secondary zone (SSZ) approximation, which is somewhat of a misnomer because averaging over an ensemble of secondary reaction zones does include the motion of the secondary reaction zone effectively.

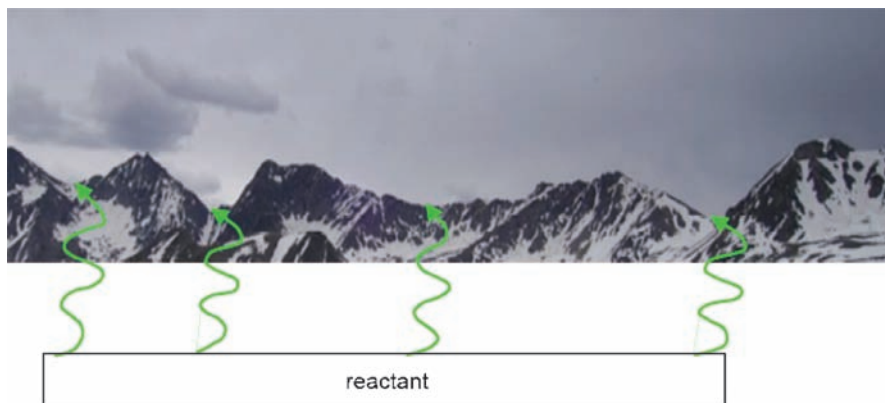


**Figure 3.3** In liquids, amorphous materials, or enzymes there is an ensemble of reaction valleys and saddle points. We average over an ensemble of these valleys; each has its own reaction coordinate.

An EA-VTST/MT calculation with the SSZ approximation is carried out in two stages. Full details of these calculations are provided in refs 38–40, and they are reviewed in refs 2–4. Here, we provide an overview.

In the first stage (which is quasiclassical, by which we mean that the reaction coordinate at the transition state is treated classically but bound vibrations are treated quantum mechanically), one selects a nonoptimised reaction coordinate, called the distinguished reaction coordinate  $z$ , and carries out a VTST calculation (in particular a CVT calculation) with this reaction coordinate, with primary reaction zone quantised (by using quantised vibrational partition functions), and with all atoms of both the primary and secondary reaction zones unfrozen. A classical-mechanical simulation is carried out to obtain a one-dimensional classical-mechanical PMF (a one-dimensional PMF is the free energy with one coordinate, the control variable or reaction coordinate  $z$ , fixed, with the PMF being a function of that variable). Using the relation<sup>98</sup> between the PMF and the free energy of activation, one may then compute a stage-1 classical mechanical free energy of activation profile. In step 2 of stage 1, one adds the difference<sup>115</sup> between the quantised vibrational free energy and the classical vibrational free energy to obtain a stage-1 quasiclassical free energy of activation profile. This is called quasiclassical because the reaction coordinate is still classical at the transition state, although the quantised vibrational step converts the treatment of all other vibrational coordinates at the transition state and all vibrational coordinates at the reactant to a quantised form. This leads to a stage-1 rate constant that may also be called a single-reaction-coordinate rate constant, that is given by

$$k^{(1)} = \frac{k_B T}{h} \exp\left(-\Delta G_T^{(1)} / RT\right) \quad (3.30)$$

where  $\Delta G_T^{(1)}$  is the stage-1 approximation to the quasiclassical free energy of activation;  $k^{(1)}$  may also be called the single-reaction-coordinate approximation

to the quasiclassical rate constant. Note that  $\Delta G_T^{(1)}$  is a quasithermodynamic quantity in that it includes no contributions from a transmission coefficient.

By sampling the variationally optimised transition-state ensemble of stage 1, one finds an ensemble of  $I$  optimised saddle points and reaction paths, which are calculated with a static secondary reaction zone. The SSZ quasiclassical rate constant is then given by

$$k^{\text{QC}} = \Gamma(T) k^{(1)} \quad (3.31)$$

and

$$\Gamma = \frac{\sum_{i=1}^I \Gamma_i(T)}{I} \quad (3.32)$$

where each  $\Gamma_i$  corrects the stage-1 rate constant for the recrossing that is eliminated by using optimised reaction coordinate  $i$ . Since reaction-coordinate motion is still classical,  $k^{\text{QC}}$  is still quasiclassical, and in fact if one stops at stage 2, it is the final estimate of the EA-VTST quasiclassical rate constant. In practice, each  $\Gamma_i(T)$  is computed from a new variational transition-state calculation with its own reaction path. Thus, one is now averaging not just over the valley associated with a single reaction path but over an ensemble of reaction paths. Thus fluctuations of the primary reaction zone are included directly in the reaction-path dynamics, and fluctuations of the secondary reaction zone are contained in the ensemble average over reaction paths.

In the second (final) step of stage 2 one includes tunnelling and nonclassical reflection for each reaction path, leading to a tunnelling transmission coefficient  $\Gamma_i$ . The rate constant is now calculated as

$$k^{\text{EA-VTST/MT}} = \gamma(T) k^{(1)}(T) \quad (3.33)$$

where

$$\gamma = \frac{\sum_{i=1}^I \kappa_i(T) \Gamma_i(T)}{I} \quad (3.34)$$

Full computational details of SSZ calculations are given elsewhere.<sup>38,39</sup>

One can also add an additional stage (stage 3) of calculation where the free-energy change due to motion of the secondary reaction zone is added as a function of progress along each reaction coordinate. This is called the equilibrium secondary zone (ESZ) approximation. Full computational details are given elsewhere.<sup>38,40</sup>

An important difference between gas-phase and condensed-phase or enzyme-catalysed reactions is the size of the system. Inclusion of solvent, an enzyme, or both results in systems of thousands of atoms. Furthermore, ensemble

averaging over configurations sampled from a canonical ensemble is essential for reliable results.<sup>1</sup> Quantum-mechanical electronic-structure calculations with appropriate averaging on systems of such size are only feasible with highly simplified methods such as those employing neglect of diatomic differential overlap.<sup>116,117</sup> The currently state-of-the-art way around this problem is to use the combined QM/MM approach,<sup>1,118–129</sup> in which a quantum-mechanical (QM) level is used to describe a small fragment of the system vital to reactivity, and a molecular-mechanics (MM) level of description is used for the remaining, bulk part (solvent, bath, or enzyme). This division into parts treated by different theory levels need not be the same as the division into primary and secondary reaction zones for dynamics.

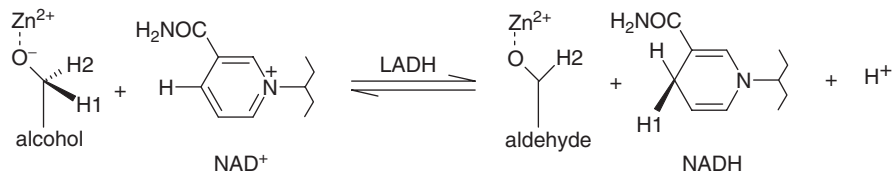
The EA-VTST/OMT method can provide detailed insight into mechanisms of enzyme-catalysed reactions. In the remaining part of this chapter, examples of applications of the EA-VTST/OMT to enzymatic systems will be presented. Four such systems were chosen to be presented with regard to their nonclassical behaviour.

### 3.3 Examples

#### 3.3.1 Liver Alcohol Dehydrogenase – A Workhorse for Studying Hydride Transfer

One of the most extensively studied groups of enzymes are those from the alcohol dehydrogenases family. One of these enzymes that has been examined thoroughly both experimentally<sup>130–143</sup> and theoretically<sup>38,144–163</sup> is liver alcohol dehydrogenase (LADH). It catalyses the reversible conversion of an alcohol to an aldehyde by transferring hydride from the substrate to the cofactor (nicotinamide adenine dinucleotide, abbreviated  $\text{NAD}^+$ ) as shown in Scheme 3.1. LADH is a metalloenzyme containing two Zn ions. One of them plays a structural role and the other is catalytically important because it interacts with the initial alcohol and the final aldehyde oxygen atoms, respectively.

Although the rate of ethanol dehydrogenation in wild-type LADH is limited by release of the product<sup>130–132</sup> the chemical step may be ‘unmasked’ in the kinetics by changing the substrate to benzyl alcohol or *para*-substituted benzyl



**Scheme 3.1** The postulated mechanism for LADH-catalysed reaction. H1 and H2 denote primary and secondary hydrogen, respectively. (Do not confuse the secondary hydrogen H2 with the  $\text{C(O)NH}_2$  amide group.)

alcohols and by mutagenesis at hydrophobic residues surrounding the active-site binding pocket.<sup>135</sup> The general conclusion drawn from a series of studies by Klinman and coworkers is that the chemical step in alcohol dehydrogenation catalysed by the wild-type LADH, mutant LADH, and yeast alcohol dehydrogenase involves a significant amount of tunnelling<sup>164</sup> but it is sometimes masked by kinetic complexity. Observed primary kinetic isotope effects (KIEs) for the hydride-transfer step in various alcohol dehydrogenase transformations of benzyl alcohol and *para*-substituted benzyl alcohols are  $k_{\text{H}}/k_{\text{D}} = 3.7\text{--}4.7$  and  $k_{\text{H}}/k_{\text{T}} = 7.0\text{--}7.8$ . In the case of secondary KIEs these values are 1.2–1.3 and 1.3–1.4, respectively.<sup>133,135,136,165</sup> Klinman and coworkers inferred significant tunnelling contributions to the process primarily from two observations. Firstly, the exponent,  $\alpha$  defined as  $\alpha = \ln(k_{\text{H}}/k_{\text{T}})/\ln(k_{\text{D}}/k_{\text{T}})$  from the Swain–Schaad relationship<sup>166</sup> was found to be in the range 4–10,<sup>125,129,145</sup> whereas values around 3.34 are usually assumed to be the upper limit in the absence of tunnelling.<sup>167</sup> Secondly, the ratio of Arrhenius pre-exponential factors  $A_{\text{H}}/A_{\text{T}}$  for the primary KIE was observed<sup>133</sup> to have a value as low as 0.5, whereas a value below 0.6 is again considered the lower limit in the absence of tunnelling.<sup>168</sup>

EA-VTST/MT was tested against the reaction dynamics taking place in the LADH active site.<sup>38,145</sup> Both the SSZ and ESZ approximations were used. These studies showed that the elevated Swain–Schaad exponents for the secondary KIEs can be obtained when quantum-tunnelling effects are included in the computation of the rate constants, but not otherwise, confirming that the large Swain–Schaad exponent for the secondary KIEs is experimental evidence for hydrogen tunnelling in LADH catalysis. It was also found that coupled motion of the secondary hydrogen in the reaction coordinate is critical for interpreting the observed secondary KIEs. The results obtained are compared to experimental data in Table 3.1. It is particularly striking that the calculations can reproduce both the primary and secondary kinetic isotope effects quite well because earlier tunnelling models<sup>169</sup> were unable to do that with realistic potential-energy surfaces. Analysis<sup>145</sup> of the multidimensional tunnelling calculations showed significant contribution to the kinetic isotope effects from isotope-dependent effective barrier widths and an isotope-dependent extent of corner cutting, neither of which is present in one-dimensional tunnelling models. (See Figure 4 in ref. 145 and associated discussion.)

### 3.3.2 Dihydrofolate Reductase – A Paradigmatic System

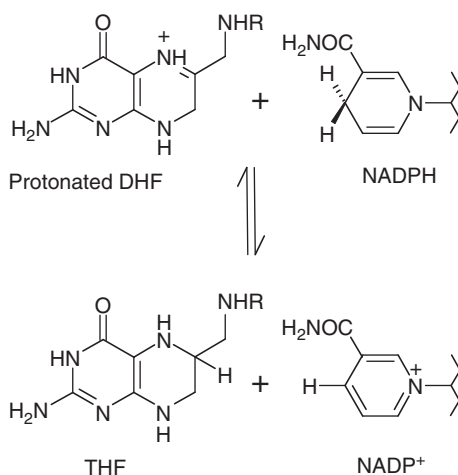
Dihydrofolate reductase (DHFR) catalyses the conversion of 7,8-dihydrofolate (DHF) to 5,6,7,8-tetrahydrofolate (THF) using reduced nicotinamide adenine dinucleotide phosphate (NADPH) as a cofactor (Scheme 3.2). To an extent that is better documented than for any other enzyme, this small protein adopts different conformations during the catalytic cycle,<sup>170–187</sup> and the impact of these conformations on the hydride-transfer step has become a platform for numerous theoretical studies.<sup>99,188–216</sup>

**Table 3.1** Primary and secondary KIEs and Swain–Schaad exponents for the reaction of benzyl alcoholate with  $\text{NAD}^+$ , catalysed by LADH, to form benzaldehyde and reduced nicotinamide adenine dinucleotide (abbreviated NADH) at 298 K.

		$EA-CVT/\mu OMT^a$		Experiment <sup>b</sup>
		SSZ	ESZ	
Primary	$k_H/k_D$	4.6	5.6	$3.8 \pm 0.7$
	$k_H/k_T$	6.9	7.5	7.1
	$k_D/k_T$	1.8	1.7	$1.9 \pm 0.01$
Secondary	$k_H/k_T$	1.26	1.36	1.33
	$k_D/k_T$	1.05	1.08	1.07
Exponent	$\alpha_{\text{prim}}$	3.3	3.6	3.1
	$\alpha_{\text{sec}}$	5.0	4.2	4.1

<sup>a</sup>Alhambra *et al.* 2001 (ref. 38)

<sup>b</sup>Bahnson *et al.* 1993, Bahnson and Klinman 1995 (refs 133,135)



**Scheme 3.2** The hydride-transfer reaction catalysed by DHFR.

At high pH rate-determining step is the transfer of a hydride ion from a carbon atom of NADPH to a carbon atom of protonated DHF; see Scheme 3.2. *E. coli* DHFR originally provided an opportunity to compare theory<sup>197</sup> and experiment<sup>217</sup> for the primary H/D KIE, and good agreement was obtained (theory: 2.8; experiment: 3.0). At the same time, a large quantum effect was predicted for the as-yet-unmeasured secondary H/D KIE. In particular, a nontunnelling calculation yielded a 3% effect, whereas including multi-dimensional tunnelling raised this to 13%. After this result was published,<sup>197</sup> the value was independently inferred from new experiments to be 13%.<sup>179</sup> This is a rare case where theory made a prediction prior to the experiments, and the success of theory for this case is very encouraging.

**Table 3.2** Primary and secondary deuterium KIEs ( $k_{\text{H}}/k_{\text{D}}$ ) for the hydride-transfer reaction catalysed by *E. coli* DHFR at 278, 298 and 318 K.

Temperature (K)	Calculated <sup>a</sup>		Experimental <sup>b</sup>	
	Primary	Secondary	Primary	Secondary
278	3.22		3.54 ± 0.16	
298	2.83 <sup>c</sup>	1.13 <sup>c</sup>	3.50 ± 0.20	1.13
318	3.01		3.58 ± 0.15	

<sup>a</sup>results from ref. 207 at 278 and 318 K

<sup>b</sup>results from ref. 179

<sup>c</sup>results from the earlier report<sup>197</sup>

Both primary and secondary H/D KIEs and their temperature dependence have been measured<sup>179</sup> for the *E. coli* DHFR. The results were interpreted in terms of environmentally coupled tunnelling and vibrationally enhanced ground-state tunnelling, where the modulation of the tunnelling amplitude by a gated motion varies with temperature. No coupling between primary and secondary hydrogen positions was observed, contrary to what had been observed for alcohol dehydrogenase.<sup>164,218</sup> Calculations using EA-VTST/MT with a combined QM/MM potential reproduced the observed weak temperature dependence of the KIEs as well as agreeing with their magnitude.<sup>207</sup> The results are compared to the original experimental data<sup>179</sup> in Table 3.2; later experiments<sup>181</sup> showed somewhat smaller pH-dependent KIEs.

Two interesting features have been identified from the theoretical temperature-dependent studies. First, there is a transition-state shift along the reaction coordinate when the temperature is changed; this shift partly cancels the temperature dependence that would be expected for the KIE in calculations with a temperature-independent effective barrier. The second interesting feature is an unusual temperature dependence of the width of the effective potential barrier for tunnelling. The EA-VTST/MT calculations including these effects predict a KIE that changes only by 6.5% over the temperature range from 278 K to 318 K, which is only slightly larger than the experimental uncertainty of the KIE. Without these two mechanisms, the KIE would have decreased by 16%. The experimentally found kinetic isotope effect for the Arrhenius pre-exponential factors of  $4.0 \pm 1.5$ <sup>179</sup> was reproduced qualitatively using the above calculation framework (1.9). The authors of the later experiments<sup>181</sup> that showed a dependence on pH concluded that their results suggested that “the mechanism by which H transfer in DHFR is coupled to protein fluctuations depends on the pH of the environment”. They also concluded, in light of the two competing temperature effects uncovered in the theoretical<sup>197</sup> studies that “it is perhaps not surprising that in such a system the temperature dependence varies with reaction conditions”.

Primary H/D KIEs have also been measured for the hydride-transfer step catalysed by the hyperthermophilic *Thermotoga maritima* DHFR (TmDHFR) within the 279–338 K temperature range; biphasic behaviour has been observed with the breakpoint at approximately 298 K.<sup>174</sup> The temperature-independent

KIEs observed in this study for higher temperatures were interpreted as indicating that tunnelling is not modulated by the environment or that such a contribution is very small. Below 298 K the observed H/D kinetic isotope effect becomes inverse, and the difference between the activation energies for protonated and deuterated substrates increases. This may suggest an increased role of active-site dynamics that alters the distance at which hydrogen is transferred. TmDHFR is therefore a good system for testing the environmentally coupled tunnelling hypothesis, and EA-VTST/MT studies were carried out<sup>210</sup> based on the same combined QM/MM potential energy parameters as employed earlier<sup>197</sup> for *E. coli* DHFR. The PMF profiles were computed at 278, 298, and 338 K for the wild-type homodimer enzyme. In addition, in order to shed light on the effect of the dimerisation on the enzyme activity, a simulation was carried out at 298 K where only the protein monomer was included. The calculated H/D primary KIEs from these simulations are compared to the experimental data in Table 3.3.

Since TmDHFR exists as a homodimer, which is believed to be mainly responsible for its thermal stability being higher than that of other DHFRs, which are monomeric, the catalytic reaction was simulated at 298 K for both the dimer and for the experimentally inaccessible monomer.<sup>210</sup> The free energy of activation was found to be 3.4 kcal/mol lower for the dimer, indicating that dimerisation is important not only for stability but for catalysis. Of the 3.4 kcal/mol enhancement, 2.6 kcal/mol can be accounted for classically so the enhancement is mainly classical with a 0.8 kcal/mol quantum contribution, primarily from quantised vibrations. In light of this finding at 298 K, all temperature-dependent studies were carried out on the dimer.<sup>210</sup>

Significant changes in the PMF barrier shape and shift of the of the locations of variational transition states were observed (see Figure 3.4) at different temperatures, similar to the shifts that partly explained the weakly temperature-dependent KIE in *E. coli* DHFR. The standard deviations of the tunnelling, recrossing and overall transmission coefficients turned out to be smaller at high temperature than at low temperature. A similar temperature-dependent behaviour of the transmission coefficients has also been observed in the *E. coli* DHFR system.<sup>207</sup> Viewing these deviations as a reflection of fluctuations of the dynamical barrier, the obtained results might suggest that at high temperature the system tunnels through more rigid barriers, which fluctuate less significantly than those at low temperatures.

**Table 3.3** Primary KIEs for the hydride-transfer reaction catalysed by TmDHFR at 278, 298 and 338 K.

Temperature (K)	$k_H/k_D$ calculated	$k_H/k_D$ experimental
278	3.0	6.7
298	2.9 (2.5) <sup>a</sup>	4.0
338	2.2	3.4

<sup>a</sup>Value in parentheses for monomer; other calculated values and experiment are for the dimer.

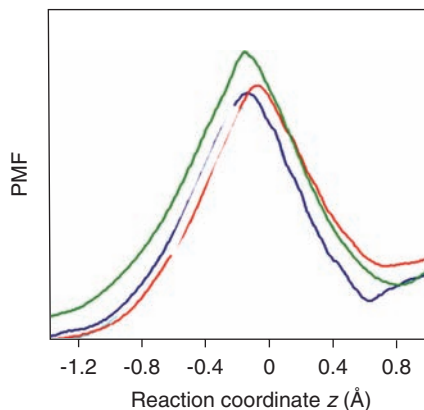
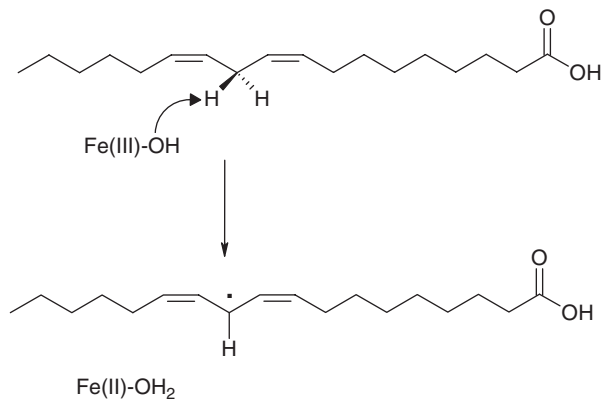


**Figure 3.4** The computed classical mechanical PMF (in kcal/mol) *vs.*, the reaction coordinate for dimeric TmDHFR at 278 K (blue line), 298 K (orange line), and 338 K (light blue line).

### 3.3.3 Soybean-Lipoxygenase-1 and Methylmalonyl-CoA Mutase – Enzymes Catalysing Hydrogen Atom Transfer Reactions that Exhibit the Largest KIEs Reported for any Biological System

Soybean lipoxygenase-1 (SLO1) is a nonheme iron enzyme that catalyses the oxidation of linoleic acid. The chemical step is a net hydrogen-atom transfer (Scheme 3.3). This enzymatic reaction has been of great interest to both experimentalists and theoreticians for the last 15 years.<sup>156,164,209,219–243</sup> One reason for the intense study of this enzymatic reaction is the large value of the experimental deuterium KIE, in particular  $k_{\text{H}}/k_{\text{D}}$  is found to be greater than 80 at 303 K. This large kinetic isotope effect is accompanied by a weak temperature dependence for both  $k_{\text{cat}}$  and its KIE over the 278–323 K temperature range.<sup>228–229,233,240</sup> This large KIE is clear evidence for extensive hydrogen tunnelling in this system, and it is very interesting to understand both the magnitude of the KIE and how such a large KIE can have such a small temperature dependence.

Several approaches<sup>156,224,227,234–243</sup> have been used to describe atomistic aspects of the SLO1 reaction. Some of the methods do not include the protein environment explicitly and others are based on combined QM/MM schemes.<sup>156,237,242,243</sup> Two groups have studied the SLO1-catalysed reaction by employing VTST/MT. Hillier and coworkers<sup>156</sup> obtained an activation energy of 6.9 kcal/mol and a KIE of 18.9 at 300 K by using the SCT approximation. However, their results are based on only one reactive configuration (which is thought to be representative of the overall average, or most common pathway, in view of the generally good agreement of the calculated properties with experiment), and that is too small a sample for reliable rate calculations. Very recently, Tejero *et al.*<sup>242</sup> have reported QM/MM-based EA-VTST/MT results for hydrogen abstraction from linoleic acid by the Fe(III)-OH cofactor in soybean

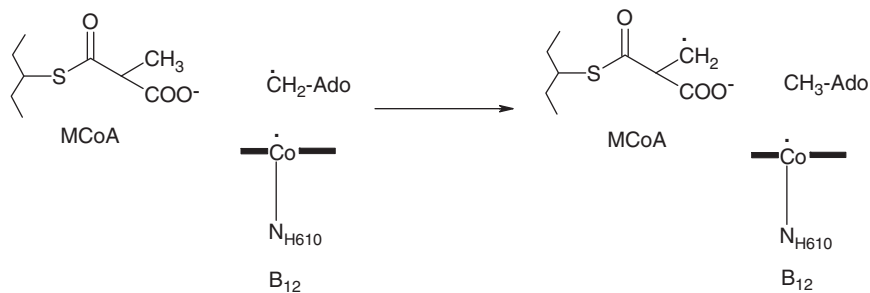


**Scheme 3.3** Hydrogen abstraction step in the reaction catalysed by SLO1 with the Fe(III)-OH cofactor.

lipoygenase-1. Although a correction had to be applied to the potential-energy barrier in order to reproduce the enormous experimental KIE, the huge contribution of tunnelling was confirmed and correlated with the width of the effective potential-energy barrier for tunnelling. This barrier is particularly narrow because of the compression of the substrate binding pocket by bulky leucine and isoleucine side chains. By comparing the results obtained for the wild-type enzyme with those for the Ile553Ala mutant, it was shown that, in the case of the mutant, the substrate-binding pocket is more expanded. The replacement of the bulky isoleucine residue with a small alanine removes the compression and rigidity observed in the wild-type enzyme. Different binding pocket flexibility leads to different barrier widths and therefore different values for KIEs.

Another example of a catalysed reaction exhibiting large involvement of tunnelling in the catalytic step is B<sub>12</sub>-dependent methylmalonyl-CoA mutase (MMCM). MMCM catalyses the rearrangement of methylmalonyl-CoA (MCoA) to succinyl-CoA. An anomalously large KIE, in particular 50 at 278 K, has been observed for the hydrogen-atom transfer from the substrate to the 5'-deoxyadenosyl radical (dAdo) in the step that initiates the isomerisation reaction in the enzyme.<sup>244</sup> The key reaction is a hydrogen radical transfer as illustrated in Scheme 3.4.

Several attempts have been made in order to elucidate the mechanism of the initial events in the MMCM-catalysed cycle. TST calculations including multidimensional tunnelling contributions performed on model systems<sup>245,246</sup> yielded primary KIEs at 293 K of 32–94, depending on the PES and model system. Although these results seem to be in reasonable agreement with the experimental primary KIE of 36 at this temperature, they do not allow for a detailed picture of the tunnelling dynamics taking place in the active site of the enzyme. Since the experience on this system indicates that only inclusion of a substantial part of the enzyme environment yields results that are pertinent to the enzyme-catalysed reaction,<sup>247</sup> EA-VTST/MT calculations were carried



**Scheme 3.4** Hydrogen-atom transfer from substrate to cofactor in the mutase-catalysed reaction. Ado- $\dot{\text{C}}\text{H}_2$  denotes the 5'-deoxyadenosyl radical, and Ado- $\text{CH}_3$  denotes 5'-deoxyadenosine. The corrin ring of vitamin B<sub>12</sub> is shown as a thick horizontal line, and the side chain of the ring is not shown, to avoid crowding in the illustration. Histidine-610 is the most important amino acid because it serves as the lower axial ligand of cobalt.

out<sup>248</sup> employing a combined quantum-mechanical and molecular-mechanical (QM/MM) potential-energy surface with unrestricted<sup>249</sup> AM1.<sup>116</sup> The calculations show that in the absence of tunnelling, the kinetic isotope effect at 278 K would only be 14. When tunnelling is included the calculated kinetic isotope effect is increased to 51 at 278 K, in excellent agreement with experiment. This provides confidence in the detailed dynamic picture of the reactive events that is afforded by the computer simulation.

Because the final results of the quantum-mechanical atomistic simulation agree with experiment so well, it is possible to analyse the nature of the tunnelling events. It was found that the tunnelling of H or D is strongly coupled to motions of the other atoms in the active site of the enzyme, and the geometrical configuration at the critical configuration of the tunnelling process was identified.

It is interesting to compare the transmission coefficients for the various members of the transition state ensemble, and this is done in Table 3.4, which contains previously unpublished details of calculations reported elsewhere.<sup>248</sup> The standard deviations of the transmission coefficients given in Table 3.4 are small compared to the effect of reaction-path curvature, indicating that the participation of fluctuating coordinates in the tunnelling path is dominated by the coordinates in the primary reaction zone, not the fluctuations of the rest of the substrate, coenzyme and protein. A special treatment near the saddle point was used that resulted in the recrossing transmission factors  $\Gamma$  being equal to unity; thus the only contribution to  $\gamma$  in this case is due to  $\kappa$ .

### 3.3.4 Other Systems and Perspectives

We will not consider other systems in detail, but rather just give a brief set of pointers to some particularly relevant literature. A more comprehensive survey of transmission coefficients with a considerable emphasis on tunnelling and coverage of a greater number of systems is given in another review<sup>250</sup> that also includes data similar to that in Table 3.4 for several other reactions. An earlier

**Table 3.4** Individual  $\kappa$  factors, for the MMCM-catalysed reaction at 278 K.

	$CH_3$				$CD_3$			
	ZCT	SCT	LCT	$\mu OMT$	ZCT	SCT	LCT	$\mu OMT$
1	12.1	81.1	54.4	83.2	7.7	21.7	16.2	22.8
2	12.9	80.2	76.2	91.4	7.7	22.6	23.9	25.7
3	11.5	71.8	65.2	86.2	8.0	24.7	16.4	23.6
4	8.8	43.0	90.3	94.4	5.8	23.6	20.0	21.9
5	13.5	82.4	57.7	83.6	9.1	30.4	17.5	30.4
6	14.0	88.4	68.4	95.3	9.0	26.0	19.2	27.6
7	14.9	93.4	54.1	93.5	9.9	29.6	18.2	30.0
8	13.2	92.3	89.9	118.0	8.3	25.2	21.8	28.5
Average	12.6	79.1	69.5	93.2	8.2	25.5	19.2	26.3
SD <sup>a</sup>	1.9	16.2	14.7	11.0	1.2	3.1	2.7	3.3

<sup>a</sup>Standard deviation

review<sup>1</sup> on the incorporation of quantum mechanics in the theoretical treatment of enzyme kinetics covers both the use of QM/MM potential-energy surfaces and also the inclusion of quantum-mechanical effects in the simulation of the dynamics; again the coverage of other systems is broad.

Three reviews of transition-state theory in general that include sections covering EA-VTST/MT are available,<sup>4,37,77</sup> and two reviews specifically devoted to EA-VTST/MT are also available.<sup>2,3</sup> The latter<sup>3</sup> of these includes a table summarising quantum effects on the phenomenological free energy of activation for several enzyme-catalysed reactions;<sup>38–40,145,197,251–253</sup> Table 3.5 extends this table to also include the methylmalonyl-CoA mutase reaction<sup>248</sup> discussed in Section 3.3.3. The reactions in Table 3.5 are all hydrogen-transfer reactions, that is, reactions in which a proton, hydride ion, or hydrogen radical is transferred. The basis for Table 3.5 is explained next.

In general we may write the rate constants, *i.e.* the experimental rate constant or the final result of a calculation, as

$$k = \frac{k_B T}{h} \exp[-\Delta G_{\text{act}}(T)/RT] \quad (3.35)$$

where  $\Delta G_{\text{act}}$  is called the phenomenological free energy of activation. Experimental results for  $k_{\text{cat}}$  are often reported as  $\Delta G_{\text{act}}$  rather than (or in addition to) reporting  $k$  itself. Equation (3.35) may also be applied to theoretical data. For example, applying it to eqns (3.31) and (3.33) and using eqn (3.30) yields

$$\Delta G_{\text{act}}^{\text{QC}} = \Delta G_T^{(1)} - RT \ln \Gamma(T) \quad (3.36)$$

and

$$\Delta G_{\text{act}}^{\text{EA-VTST/MT}} = \Delta G_T^{(1)} - RT \ln \gamma(T) \quad (3.37)$$

The difference between these two phenomenological free energies of activation is given in the “Tunnelling” column of Table 3.5. The “Quantised

**Table 3.5** Magnitudes of nuclear-motion quantum effects on phenomenological free energies of activation for enzyme-catalysed reactions.

	<i>Contribution to free energy of activation</i>			<i>Factor in rate</i>
	<i>(kcal/mol)</i>			
	<i>Ref.</i>	<i>Quantised vibrations</i>	<i>Tunnelling</i>	
Enolase	251	-2.1	-0.3	56
Alcohol dehydrogenase	38,145	-1.8	-0.8	81
Methylamine dehydrogenase	252	-3.2	-2.5	15 000
Xylose isomerase	39,253	-1.3	-1.1	58
Dihydrofolate reductase	197	-1.6	-0.6	41
Acyl-CoA dehydrogenase	40	-3.1	-0.8	720
Methylmalonyl-CoA mutase <sup>a</sup>	248	-2.2	-2.5	5100
Average		-2.2	-1.2	320 <sup>b</sup>

<sup>a</sup>This row is for 278 K; all other rows are for 298 K.

<sup>b</sup>This is computed from the sum of the averages in the two previous columns.

vibrations” column of Table 3.5 is similarly obtained by comparing  $\Delta G_{\text{act}}^{\text{QC}}$  to the free energy of activation calculated by a stage-1 procedure where vibrations are not quantised. Both columns contain negative numbers because those quantum effects speed up the reactions in all these cases. The total speed up factor is given in the last column.

Table 3.5 shows the importance of including the quantum effects on nuclear motion in modelling enzyme-catalysed hydrogen-transfer reactions. The rate enhancements range from 41 to 15 000 and those values correspond to the free energy of activation contributions of  $-2.2$  to  $-5.7$  kcal/mol. The effect of quantising vibrations is especially important for hydrogen-transfer reactions because the frequency of the stretching vibration corresponding to the bond to the hydrogen that is about to be transferred usually decreases significantly (of the order of a factor of two) as one proceeds to the midpoint of the transfer process. Since hydrogen stretching vibrations are usually high-frequency modes ( $\sim 2500\text{--}4000\text{ cm}^{-1}$ ),<sup>254</sup> this releases a considerable amount of energy into the reaction-coordinate motion, and it can contribute significantly to lowering the effective barrier to the reaction. This effect often dominates the “Quantised vibrations” effect in Table 3.5; the “Quantised vibrations” column of Table 3.5 includes the effect of quantising all the vibrational modes, including the reaction coordinate, of the reactants but not including the reaction coordinate at the variational transition state since that is excluded from the partition functions in eqn (3.4). The effect of quantisation of the reaction coordinate of the transition state is included in the “Tunnelling” column of Table 3.5, which is labelled that way because tunnelling effects dominate  $\kappa_i$ .

The average value by which tunnelling lowers the free energy of activation is  $-1.2$  kcal/mol. Two systems presented in Table 3.5 exhibit twice as high a contribution of tunnelling: methylamine dehydrogenase and methylmalonyl-CoA

mutase. As discussed in the original references<sup>38–40,145,197,248,251–253</sup> and a review,<sup>3</sup> VTST/MT yielded good agreement with experiment for kinetic isotope effects in all of these enzyme-catalysed reactions, showing it is capable of treating reactions even with large tunnelling and quantised-vibration effects. Recent concerns<sup>255</sup> that transition-state theory is inadequate for enzyme-catalysed hydrogen transfer and that a new conceptual framework is required seem to be based mainly on a lack of appreciation of the broad applicability of transition-state concepts and the consistent way (see below) that multidimensional tunnelling has been integrated into the theory.

In addition to the study in Table 3.5,<sup>252</sup> the methylamine dehydrogenase reaction and reactions catalysed by other amine dehydrogenases have also been simulated by other groups,<sup>156,239,256–265</sup> and the reader is referred to these papers for many interesting insights into the tunnelling dynamics.

One additional study that we would like to single out for special attention is the careful VTST/MT modelling of the proton transfer in the reaction catalysed by triosephosphate isomerase by Cui and Karplus.<sup>266</sup>

Another perspective on the quantum effects on reaction–coordinate motion is to not separately calculate the result with classical reaction–coordinate motion. Then, the tunnelling contribution is included in the phenomenological free energy of activation from the very beginning, and it may be interpreted as a Heisenberg broadening of the transition-state energy levels. This interpretation is discussed in another review.<sup>113</sup> It is worth mentioning that the final result is independent of whether or not it is factored into a quasiclassical part and a tunnelling transmission coefficient. This factorisation is useful though for interpretative purposes. (For example, the ability to factor the rate constant in VTST/MT calculations allows one to analyse tunnelling contributions in a way that is not possible otherwise.<sup>267</sup>)

We conclude this section with a brief discussion of the way that transition-state quantisation affects the microcanonical rate constants in small gas-phase systems because this perspective is helpful for understanding how these effects are fully included in a consistent way in the quantised transition-state theory reviewed here. The rate constant  $k(T)$  for a canonical ensemble at temperature  $T$  may be written in terms of the rate constants  $k(E)$  for microcanonical ensemble of reactants at total energy  $E$  by the formula<sup>19,34,113</sup>

$$k(T) = \frac{\int dE \rho^R(E) \exp[-(E - V^\ddagger)/k_B T] k(E)}{\Phi^R(T)} \exp(-V^\ddagger/k_B T) \quad (3.38)$$

where  $k_B T$ ,  $\Phi^R(T)$ , and  $V^\ddagger$  have the same meaning as in eqn (3.1),  $\rho^R(E)$  is the reactants' density of states per unit energy and per unit volume, and the rate constant at energy  $E$  may be written as<sup>268,269</sup>

$$k(E) = \frac{\sum_n \sum_{n'} P_{nn'}(E)}{h \rho^R(E)} \quad (3.39)$$

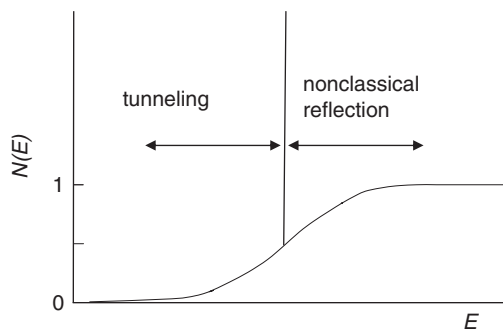


**Figure 3.5** A typical step in the cumulative reaction probability as a function of energy.

The quantity in the numerator of eqn (3.39) is called the cumulative reaction probability  $N(E)$ , and eqn (3.39) may be written as<sup>270</sup>

$$k(E) = \frac{N(E)}{h\rho^R(E)} \quad (3.40)$$

If transition-state theory were valid but the reaction-coordinate motion was classical,  $N(E)$  would be a series of unit steps at the quantised transition states. Accurate quantum-mechanical dynamics calculations show that these steps are present, are typically centred close to the energies of the maxima of the vibrationally adiabatic potential curves, and typically have close-to-unit height, but are rounded,<sup>75,76,113,269,271,272</sup> as shown for a typical step in Figure 3.5. The rounded portion on the low-energy side of the step corresponds to tunnelling, and the rounded portion on the high-energy side corresponds to nonclassical reflection. If all of these rounded steps had the same shape, the assumption introduced before eqn (3.10) would be exact. Although there are important quantitative differences in the step shapes that can be understood in terms of the effective barrier shapes presented by the excited-state vibrationally adiabatic potential curves, it turns out that many of the low-energy steps have very similar peak shapes.<sup>75,76,113,269,271,272</sup> Thus, the transmission coefficient is a very reasonable way to correct for the quantum-mechanical nature of the reaction-coordinate motion.

### 3.4 Concluding Remarks

EA-VTST/MT builds on the success of VTST/MT methods that are well validated for gas-phase reactions.<sup>4,27,37,77,273,274</sup> The theoretical studies summarised above are fully consistent with the conclusion that quantum-mechanical effects in enzyme-catalysed reactions can be understood in terms of the same principles that govern reactions in liquid-phase solution and in the gas

phase, namely quantised vibrations (including zero-point energy) and thermally activated multidimensional tunnelling.

For enzyme-catalysed reactions, quantum effects are particularly important for hydrogen transfer, that is for transfers of protons, hydride ions, and hydrogen radicals. It has been shown that quantised vibrations and quantum-mechanical tunnelling can both be included based on a reaction coordinate that is dominated by the coordinates of the breaking and forming bonds, and quantum-mechanical effects are included in transition-state theory for enzyme-catalysed reactions in the same way as for simple gas-phase reactions, by quantising vibrational motions in phase space and by a transmission coefficient that includes quantal transmission through the same barriers that control overbarrier thresholds. Enzyme-catalysed hydrogen-transfer reactions are usually electronically adiabatic. The extra complexity of enzymes and coenzymes contributes in three ways: (i) an ensemble of reaction paths corresponding to a distribution of protein conformational states must be considered; (ii) there are many degrees of freedom coupled to the substrate component of the reaction coordinate, and a great variety of coupling mechanisms are possible; (iii) the importance of biological reactions and their consequent study as catalysed by a myriad of wild-type and mutated enzymes has uncovered a cornucopia of fascinating variations on the central paradigm, each with its own nuances.

## Appendix – Quantum-Mechanical Rate Theory

This appendix contains a few comments about how one would treat reactive rate constants by exact quantum mechanics. Although converged quantum-mechanical calculations are impractical for enzyme reactions, consideration of the formalisms for converged calculations adds perspective. To calculate an accurate rate constant in the gas phase one first calculates reaction cross sections<sup>275</sup> by quantum-mechanical scattering theory.<sup>275–279</sup> By averaging these over a Maxwell–Boltzmann distribution of collision energies and a Boltzmann distribution of internal states, one then obtains reaction rate constants.<sup>280,281</sup> Accurate rates may also be calculated directly from flux correlation functions.<sup>282–286</sup> In a liquid, only the flux correlation function method remains applicable, and a variety of formulations is possible.<sup>287–292</sup> The relationship of transition-state theory to the accurate flux correlation function approach is discussed elsewhere.<sup>12,283,288,290</sup>

## Acknowledgments

This work was supported in part by the National Science Foundation under grant no. CHE07-04974.

## References

1. J. Gao and D. G. Truhlar, *Annu. Rev. Phys. Chem.*, 2002, **53**, 467.

2. D. G. Truhlar, J. Gao, C. Alhambra, M. Garcia-Viloca, J. Corchado, M. L. Sánchez and J. Villà, *Acc. Chem. Res.*, 2002, **35**, 341.
3. D. G. Truhlar, J. Gao, M. Garcia-Viloca, C. Alhambra, J. Corchado, M. L. Sanchez and T. D. Poulsen, *Int. J. Quantum Chem.*, 2004, **100**, 1136.
4. D. G. Truhlar, in *Isotope Effects in Chemistry and Biology*, ed. A. Kohen and H.-H. Limbach, Taylor & Francis, Boca Raton, FL, 2006, pp. 579–619.
5. A. Dybala-Defratyka, P. Paneth, R. Banerjee and D. G. Truhlar, *Proc. Natl. Acad. Sci. USA*, 2007, **104**, 10774.
6. H. Eyring, *J. Chem. Phys.*, 1935, **3**, 107.
7. E. Wigner, *Trans. Faraday Soc.*, 1938, **34**, 29.
8. H. Eyring, *Trans. Faraday Soc.*, 1938, **34**, 41.
9. M. G. Evans, *Trans. Faraday Soc.*, 1938, **34**, 51.
10. S. Glasstone, K. J. Laidler and E. Eyring, *The Theory of Rates Processes*, McGraw-Hill, New York, 1941.
11. H. S. Johnston, *Gas-Phase Reaction-Rate Theory*, Ronald Press, New York, 1966.
12. D. G. Truhlar, W. L. Hase and J. T. Hynes, *J. Phys. Chem.*, 1983, **87**, 2664.
13. D. G. Truhlar, B. C. Garrett and S. J. Klippenstein, *J. Phys. Chem.*, 1996, **100**, 12771.
14. M. Garcia-Viloca, J. Gao, M. Karplus and D. G. Truhlar, *Science*, 2004, **303**, 186.
15. J. C. Keck, *Adv. Chem. Phys.*, 1967, **13**, 85.
16. B. H. Mahan, *J. Chem. Educ.*, 1974, **52**, 709.
17. S. C. Tucker and D. G. Truhlar, in *New Theoretical Concepts for Understanding Organic Reactions*, ed. J. Bertrán and I. G. Csizmadia, Kluwer, Dordrecht, 1989, pp. 291–346.
18. D. G. Truhlar and B. C. Garrett, *Acc. Chem. Res.*, 1980, **13**, 440.
19. B. C. Garrett and D. G. Truhlar, *J. Phys. Chem.*, 1979, **83**, 1079. Erratum: 1983, **87**, 4553.
20. D. G. Truhlar, A. D. Isaacson, R. T. Skodje and D. G. Truhlar, *J. Phys. Chem.*, 1982, **86**, 2252.
21. D. G. Truhlar, *J. Chem. Phys.*, 1972, **56**, 3189. Erratum: 1974, **61**, 440.
22. E. Wigner, *Z. Physik. Chem.*, 1932, **B19**, 203.
23. R. P. Bell, *Trans. Faraday Soc.*, 1959, **55**, 1.
24. D. G. Truhlar and A. Kuppermann, *Chem. Phys. Lett.*, 1971, **9**, 269.
25. R. A. Marcus and M. E. Coltrin, *J. Chem. Phys.*, 1977, **67**, 2609.
26. D. G. Truhlar and B. C. Garrett, *Annu. Rev. Phys. Chem.*, 1984, **35**, 159.
27. T. C. Allison and D. G. Truhlar, in *Modern Methods for Multidimensional Dynamics Calculations in Chemistry*, ed. D. L. Thompson, World Scientific, Singapore, 1998, pp. 618–712.
28. A. Fernandez-Ramos, B. A. Ellingson, B. C. Garrett and D. G. Truhlar, in *Reviews in Computational Chemistry*, ed. K. B. Lipkowitz and T. R. Cundari, Wiley-VCH, Hoboken, NJ, 2007, pp. 125–232.
29. B. C. Garrett, D. G. Truhlar, R. S. Grev and A. W. Magnuson, *J. Phys. Chem.*, 1980, **84**, 1730. Erratum: 1983, **87**, 4554.

30. D. G. Truhlar, Y.-P. Liu, G. K. Schenter and B. C. Garrett, *J. Phys. Chem.*, 1994, **98**, 8396.
31. E. Wigner, *J. Chem. Phys.*, 1937, **5**, 720.
32. J. Horiuti, *Bull. Chem. Soc. Japan*, 1938, **13**, 210.
33. B. C. Garrett and D. G. Truhlar, *J. Chem. Phys.*, 1979, **70**, 1593.
34. B. C. Garrett and D. G. Truhlar, *J. Phys. Chem.*, 1979, **83**, 1052. Erratum: 1983, **87**, 4553.
35. G. K. Schenter, B. C. Garrett and D. G. Truhlar, *J. Phys. Chem. B*, 2001, **105**, 9672.
36. P. G. Bolhuis, C. Dellago and D. Chandler, *Faraday Discuss.*, 1998, **110**, 421–482.
37. B. C. Garrett and D. G. Truhlar, in *Theory and Applications of Computational Chemistry: The First Forty Years*. ed. C. E. Dykstra, ed. C. E. Dykstra, G. Frenking, K. S. Kim and G. E. Scuseria, Elsevier, Amsterdam, 2005, pp. 67–87.
38. C. Alhambra, J. Corchado, M. L. Sánchez, M. Garcia-Viloca, J. Gao and D. G. Truhlar, *J. Phys. Chem. B*, 2001, **105**, 11326.
39. M. Garcia-Viloca, C. Alhambra, D. G. Truhlar and J. Gao, *J. Comput. Chem.*, 2003, **24**, 177.
40. T. D. Poulsen, M. Garcia-Viloca, J. Gao and D. G. Truhlar, *J. Phys. Chem. B*, 2003, **107**, 9567.
41. A. Ben-Naim, *Statistical Thermodynamics for Chemists and Biochemists*, Plenum, New York, 1992, p. 38.
42. R. K. Boyd, *Chem. Rev.*, 1977, **77**, 93.
43. C. Lim and D. G. Truhlar, *J. Phys. Chem.*, 1985, **89**, 5.
44. C. Lim and D. G. Truhlar, *J. Phys. Chem.*, 1986, **90**, 2616.
45. H. Teitelbaum, *Chem. Phys.*, 1993, **173**, 91.
46. H. Teitelbaum, *Chem. Phys. Lett.*, 1993, **202**, 242.
47. J. C. Keck, *J. Chem. Phys.*, 1960, **32**, 1035.
48. R. L. Jaffe, J. M. Henry and J. B. Anderson, *J. Chem. Phys.*, 1973, **59**, 1128.
49. W. H. Miller, *J. Chem. Phys.*, 1974, **61**, 1823.
50. B. C. Garrett and D. G. Truhlar, *J. Am. Chem. Soc.*, 1979, **101**, 4534.
51. M. M. Kreevoy and D. G. Truhlar, in *Investigation of Rates and Mechanisms of Reactions*, ed. C. F. Bernasconi, John Wiley and Sons, New York, 1986, part 1, pp. 13–95.
52. K. A. Connors, in *Chemical Kinetics: The Study of Reaction Rates in Solution*, VCH Publishers, New York, 1990, p. 207.
53. M. J. Pilling and P. W. Seakins, *Reaction Kinetics*, Oxford University Press, Oxford, United Kingdom, 1995, p. 155.
54. B. C. Garrett and D. G. Truhlar, *J. Chem. Phys.*, 1982, **76**, 1853.
55. D. G. Truhlar, A. D. Isaacson and B. C. Garrett, in *Theory of Chemical Reaction Dynamics*, ed. M. Baer, CRC Press, Boca Raton, FL, 1985, pp. 65–137.
56. J. O. Hirschfelder and E. Wigner, *J. Chem. Phys.*, 1939, **7**, 616.
57. W. H. Miller, *J. Chem. Phys.*, 1976, **65**, 2216.

58. Y.-Y. Chuang, C. J. Cramer and D. G. Truhlar, *Int. J. Quantum Chem.*, 1998, **70**, 887.
59. J. Villà and D. G. Truhlar, *Theor. Chem. Acc.*, 1997, **97**, 317.
60. C. F. Jackels, Z. Gu and D. G. Truhlar, *J. Chem. Phys.*, 1995, **102**, 3188.
61. P. L. Fast and D. G. Truhlar, *J. Chem. Phys.*, 1998, **109**, 3721.
62. C. Eckart, *Phys. Rev.*, 1930, **35**, 1303.
63. C. A. Mead, in *Mathematical Frontiers in Computational Chemical Physics*, ed. D. G. Truhlar, Springer-Verlag, New York, 1988, pp. 1–17.
64. J. Simons and J. Nichols, *Quantum Mechanics in Chemistry*, Oxford University Press, New York, 1997, p. 43.
65. D. G. Truhlar, in *The Encyclopedia of Physical Science and Technology*, ed. R. A. Meyers, 3rd edn, Academic Press, New York, 2001, **Vol. 13**, pp. 9–13.
66. P. Atkins and R. Friedman, *Molecular Quantum Mechanics*, 4th edn, Oxford University Press, Oxford, 2005, p. 249.
67. R. A. Marcus, *J. Chem. Phys.*, 1966, **45**, 4500.
68. D. G. Truhlar and A. Kuppermann, *J. Chem. Phys.*, 1970, **52**, 3841.
69. D. G. Truhlar and A. Kuppermann, *J. Am. Chem. Soc.*, 1971, **93**, 1840.
70. D. G. Truhlar, *J. Chem. Phys.*, 1970, **53**, 2041.
71. J. M. Bowman, A. Kuppermann, J. T. Adams and D. G. Truhlar, *Chem. Phys. Lett.*, 1973, **20**, 229.
72. J. W. Duff and D. G. Truhlar, *Chem. Phys. Lett.*, 1973, **23**, 327.
73. D. G. Truhlar and R. E. Wyatt, *Annu. Rev. Phys. Chem.*, 1976, **27**, 1.
74. R. T. Skodje, D. G. Truhlar and B. C. Garrett, *J. Chem. Phys.*, 1982, **77**, 5955.
75. D. C. Chatfield, R. S. Friedman, D. G. Truhlar, B. C. Garrett and D. W. Schwenke, *J. Am. Chem. Soc.*, 1991, **113**, 486.
76. D. C. Chatfield, R. S. Friedman, D. G. Truhlar and D. W. Schwenke, *Faraday Discuss. Chem. Soc.*, 1991, **91**, 289.
77. D. G. Truhlar and B. C. Garrett, in *Hydrogen Transfer Reactions*, ed. J. T. Hynes, J. P. Klinman, H. H. Limbach and R. L. Schowen, Wiley-VCH, Weinheim, Germany, 2007, **Vol. 2**, pp. 833–874.
78. R. A. Marcus, *J. Chem. Phys.*, 1966, **45**, 4493.
79. R. A. Marcus, *J. Chem. Phys.*, 1968, **49**, 2617.
80. A. Kuppermann, J. T. Adams and D. G. Truhlar, in Abstracts Papers, *Int. Conf. Phys. Electron. At. Coll. Beograd*, ed. B. C. Cubic and M. V. Kurepa, Belgrade, Serbia, 1973, **8**, 149.
81. R. T. Skodje and D. G. Truhlar, *J. Phys. Chem.*, 1981, **85**, 624.
82. B. C. Garrett, D. G. Truhlar, A. F. Wagner and T. H. Dunning Jr., *J. Chem. Phys.*, 1983, **78**, 4400.
83. D. K. Bondi, J. N. L. Connor, B. C. Garrett and D. G. Truhlar, *J. Chem. Phys.*, 1983, **78**, 5981.
84. B. C. Garrett and D. G. Truhlar, *J. Chem. Phys.*, 1983, **79**, 4931.
85. M. M. Kreevoy, D. Ostovic, D. G. Truhlar and B. C. Garrett, *J. Phys. Chem.*, 1986, **90**, 3766.
86. D. G. Truhlar and B. C. Garrett, *J. Chim. Phys.*, 1987, **84**, 365.

87. D. G. Truhlar and M. S. Gordon, *Science*, 1990, **249**, 491.
88. Y. Kim, D. G. Truhlar and M. M. Kreevoy, *J. Am. Chem. Soc.*, 1991, **113**, 7837.
89. T. Taketsugu and K. Hirao, *J. Chem. Phys.*, 1997, **107**, 10506.
90. C. S. Tautermann, A. F. Voegel, T. Loerting and K. R. Leidl, *J. Chem. Phys.*, 2002, **117**, 1962.
91. B. K. Dey and P. W. Ayers, *Mol. Phys.*, 2007, **105**, 71.
92. Y. P. Liu, D.-h. Lu, A. Gonzalez-Lafont, D. G. Truhlar and B. C. Garrett, *J. Am. Chem. Soc.*, 1993, **115**, 7806.
93. A. Fernandez-Ramos and D. G. Truhlar, *J. Chem. Phys.*, 2001, **114**, 1491.
94. D.-h. Lu, T. N. Truong, V. S. Melissas, G. C. Lynch, Y.-P. Liu, B. C. Garrett, R. Steckler, A. D. Isaacson, S. N. Rai, G. C. Hancock, J. G. Lauderdale, T. Joseph and D. G. Truhlar, *Comput. Phys. Commun.*, 1992, **71**, 235.
95. Y.-P. Liu, G. C. Lynch, T. N. Truong, D.-h. Lu, D. G. Truhlar and B. C. Garrett, *J. Am. Chem. Soc.*, 1993, **115**, 2408.
96. B. C. Garrett, T. Joseph, T. N. Truong and D. G. Truhlar, *Chem. Phys.*, 1989, **136**, 271.
97. T. N. Truong, D.-h. Lu, G. C. Lynch, Y.-P. Liu, V. S. Melissas, J. J. P. Stewart, R. Steckler, B. C. Garrett, A. D. Isaacson, A. Gonzalez-Lafont, S. N. Rai, G. C. Hancock, T. Joseph and D. G. Truhlar, *Comput. Phys. Commun.*, 1993, **75**, 143.
98. G. K. Schenter, B. C. Garrett and D. G. Truhlar, *J. Chem. Phys.*, 2003, **119**, 5828.
99. J. B. Watney, A. V. Soudackov, K. F. Wong and S. Hammes-Schiffer, *Chem. Phys. Lett.*, 2006, **418**, 268.
100. E. C. Kemble, *Fundamental Principles of Quantum Mechanics with Elementary Applications*, Dover, New York, 1937.
101. J. Heading, *An Introduction to Phase Integral Methods*, Methuen, London, 1961.
102. B. C. Garrett and D. G. Truhlar, *J. Phys. Chem.*, 1979, **83**, 2921.
103. K. Gottfried and T.-M. Yan, *Quantum Mechanics: Fundamentals*, 2nd edn, Springer, New York, 2003, pp. 103, 217–228.
104. F. T. Smith, *J. Chem. Phys.*, 1965, **42**, 2419.
105. H. C. Corben and P. Stehle, *Classical Mechanics*, 2nd edn, Robert E. Krieger Publishing Co., Huntington, NY, 1960, p. 170, (a) p. 32.
106. I. M. Gelfand and S. V. Fomin, *Calculus of Variations*, Prentice-Hall, Englewood Cliffs, NJ, 1963, p. 84.
107. H. Goldstein, C. Poole and J. Safko, *Classical Mechanics*, Addison Wesley, San Francisco, 2002, pp. 353–362.
108. E. C. G. Sudarshan and N. Mukunda, *Classical Dynamics: A Modern Perspective*, John Wiley & Sons, New York, 1974, pp. 12–29.
109. E. B. Wilson Jr., J. C. Decius and P. C. Cross, *Molecular Vibrations*, Dover Publications, New York, 1955, p. 14.
110. S. Califano, *Vibrational States*, John Wiley & Sons, London, 1976, p. 21, (a) p. 256.

111. D. G. Truhlar and A. Kuppermann, *J. Chem. Phys.*, 1972, **56**, 2232.
112. L. Melander and W. H. Saunders Jr., *Reaction Rates of Isotopic Molecules*, John Wiley & Sons, New York, 1980.
113. D. C. Chatfield, R. S. Friedman, S. L. Mielke, G. C. Lynch, T. C. Allison, D. G. Truhlar and D. W. Schwenke, in *Dynamics of Molecules and Chemical Reactions*, ed. R. E. Wyatt and J. Z. H. Zhang, Marcel Dekker, New York, 1996, pp. 323–386.
114. B. C. Garrett, H. Abusalbi, D. J. Kouri and D. G. Truhlar, *J. Chem. Phys.*, 1985, **83**, 2252.
115. M. Garcia-Viloca, C. Alhambra, D. G. Truhlar and J. Gao, *J. Chem. Phys.*, 2001, **114**, 9953.
116. (a) M. J. S. Dewar, E. Zoebisch, E. F. Healy and J. J. P. Stewart, *J. Am. Chem. Soc.*, 1985, **107**, 3902; (b) J. J. P. Stewart, *J. Comp. Chem.*, 1989, **10**, 209.
117. N. G. J. Richards, in *Molecular Orbital Calculations for Biological Systems*, ed. A.-M. Sapse, Oxford University Press, New York, 1998, p. 11.
118. P. Amara, M. J. Field, C. Alhambra and J. Gao, *Theor. Chem. Acc.*, 2000, **104**, 336.
119. A. Shurki and A. Warshel, *Adv. Protein Chem.*, 2003, **66**, 249.
120. U. Ryde, *Curr. Opinion Struct. Biol.*, 2003, **3**, 136.
121. G. Tresadern, S. Nunez, P. F. Faulder, H. Wang, I. H. Hillier and N. A. Burton, *Faraday Discuss.*, 2003, **122**, 223.
122. P. Amara and M. J. Field, *Theor. Chem. Acc.*, 2003, **109**, 43.
123. J. Pu, J. Gao and D. G. Truhlar, *J. Phys. Chem. A*, 2004, **108**, 632.
124. (a) F. Claeysens, K. E. Ranaghan, F. R. Manby, J. N. Harvey and A. J. Mulholland, *Chem. Comm.*, 2005, **2005**, 5068; (b) A. J. Mulholland, *Chem. Central J.*, 2007, **1**, 19.
125. W. L. Jorgensen and J. Tirado-Rives, *J. Comp. Chem.*, 2005, **26**, 1689.
126. T. Vreven, K. S. Byun, I. Komaromi, S. Dapprich, J. A. Montgomery, K. Morokuma Jr. and M. J. Frisch, *J. Chem. Theory Comput.*, 2006, **2**, 815.
127. J. J. Ruiz-Pernia, E. Silla, I. Tuñon and S. Marti, *J. Phys. Chem. B*, 2006, **110**, 17663.
128. H. Lin and D. G. Truhlar, *Theor. Chem. Acc.*, 2007, **117**, 185.
129. H. M. Senn and W. Thiel, *Curr. Opin. Struct. Biol.*, 2007, **11**, 182.
130. P. F. Cook, J. S. Blanchard and W. Cleland, *Biochemistry*, 1980, **19**, 4853.
131. V. C. Sekhar and B. V. Plapp, *Biochemistry*, 1990, **29**, 4289.
132. G. L. Shearer, K. Kim, K. M. Lee, C. K. Wang and B. V. Plapp, *Biochemistry*, 1993, **32**, 11186.
133. B. J. Bahnson and J. P. Klinman, *Methods Enzymol.*, 1995, **249**, 373.
134. C. L. Stone, W. F. Bosron and M. F. Dunn, *J. Biol. Chem.*, 1993, **268**, 892.
135. B. J. Bahnson, D.-H. Park, K. Kim, B. V. Plapp and J. P. Klinman, *Biochemistry*, 1993, **32**, 5503.
136. B. J. Bahnson, T. D. Colby, J. K. Chin, B. M. Goldstein and J. P. Klinman, *Proc. Natl. Acad. Sci. USA*, 1997, **94**, 12797.

137. H. Deng, J. F. Schneider, K. B. Berst, B. V. Plapp and R. Callender, *Biochemistry*, 1998, **37**, 14267.
138. S. Ramaswamy, D.-H. Park and B. V. Plapp, *Biochemistry*, 1999, **38**, 13951.
139. J. K. Rubach, S. Ramaswamy and B. V. Plapp, *Biochemistry*, 2001, **40**, 12686.
140. J. K. Rubach and B. V. Plapp, *Biochemistry*, 2002, **41**, 15770.
141. B. V. Plapp, in *Isotope Effects in Chemistry and Biology*, ed. A. Kohen and H.-H. Limbach, CRC/Taylor & Francis, Boca Raton, FL, 2006, pp. 811–835.
142. Z. D. Nagel and J. P. Klinman, *Chem. Rev.*, 2006, **106**, 3095.
143. R. Meijers, H.-W. Adolph, Z. Dauter, K. S. Wilson, V. S. Lamzin and E. S. Cedergren-Zappezauer, *Biochemistry*, 2007, **46**, 5446.
144. P. K. Agarwal, S. P. Webb and S. Hammes-Schiffer, *J. Am. Chem. Soc.*, 2000, **122**, 4803.
145. C. Alhambra, J. Gao, J. C. Corchado, M. L. Sanchez and D. G. Truhlar, *J. Am. Chem. Soc.*, 2000, **122**, 8197.
146. S. Hammes-Schiffer and S. R. Billeter, *Int. Rev. Phys. Chem.*, 2001, **20**, 591.
147. S. R. Billeter, S. P. Webb, P. K. Agarwal, T. Iordanov and S. Hammes-Schiffer, *J. Am. Chem. Soc.*, 2001, **123**, 11262.
148. J. Luo and T. C. Bruice, *J. Am. Chem. Soc.*, 2001, **123**, 11952.
149. S. R. Billeter, S. P. Webb, T. Iordanov, P. K. Agarwal and S. J. Hammes-Schiffer, *J. Chem. Phys.*, 2001, **114**, 6925.
150. J. Villa and A. Warshel, *J. Phys. Chem. B*, 2001, **105**, 7887.
151. S. P. Webb, P. K. Agarwal and S. Hammes-Schiffer, *J. Phys. Chem. B*, 2001, **104**, 8894.
152. Q. Cui, M. Elstner and M. Karplus, *J. Phys. Chem. B*, 2002, **106**, 2721.
153. S. Cartzoulas, J. S. Mincer and S. D. Schwartz, *J. Am. Chem. Soc.*, 2002, **124**, 3270.
154. A. Kohen and J. H. Jensen, *J. Am. Chem. Soc.*, 2002, **124**, 3858.
155. J. Luo and T. C. Bruice, *Proc. Natl. Acad. Sci. USA*, 2002, **99**, 16597.
156. G. Tresadern, J. P. McNamara, M. Mohr, H. Wang, N. A. Burton and I. H. Hillier, *Chem. Phys. Lett.*, 2002, **358**, 489.
157. C. Kalyanoraman and S. D. Schwartz, *J. Phys. Chem. B*, 2002, **106**, 13111.
158. J. S. Mincer and S. D. Schwartz, *J. Phys. Chem. B*, 2003, **107**, 366.
159. A. Warshel and J. Villà-Friexa, *J. Phys. Chem. B*, 2003, **107**, 12370.
160. S. D. Schwartz, *J. Phys. Chem. B*, 2003, **107**, 12372.
161. G. Tresadern, P. F. Faulder, M. P. Gleeson, Z. Tai, G. MacKenzie, N. A. Burton and I. H. Hillier, *Theor. Chem. Acc.*, 2003, **109**, 108.
162. J. Luo and T. C. Bruice, *Proc. Natl. Acad. Sci. USA*, 2004, **101**, 13152.
163. J. Luo and T. C. Bruice, *Biophys. Chem.*, 2007, **126**, 80.
164. A. Kohen and J. P. Klinman, *Acc. Chem. Res.*, 1998, **31**, 397.
165. Y. Cha, C. J. Murray and J. P. Klinman, *Science*, 1989, **243**, 1325.

166. C. G. Swain, E. C. Stivers, J. E. Reuwer and L. J. Schaad, *J. Am. Chem. Soc.*, 1958, **80**, 5885.
167. W. H. Saunders, *J. Am. Chem. Soc.*, 1985, **107**, 164.
168. M. E. Schneider and M. J. Stern, *J. Am. Chem. Soc.*, 1972, **94**, 1517.
169. J. Rucker and J. P. Klinman, *J. Am. Chem. Soc.*, 1999, **212**, 1997.
170. M. R. Sawaya and J. Kraut, *Biochemistry*, 1997, **36**, 586.
171. C. J. Falzone, P. E. Wright and S. E. Benkovic, *Biochemistry*, 1994, **33**, 439.
172. M. J. Osborne, J. Schnell, S. J. Benkovic, H. J. Dyson and P. E. Wright, *Biochemistry*, 2001, **40**, 9846.
173. P. T. R. Rajagopalan, S. Lutz and B. J. Benkovic, *Biochemistry*, 2002, **41**, 12618.
174. G. Maglia and R. K. Allemann, *J. Am. Chem. Soc.*, 2003, **125**, 13372.
175. P. Shrimpton, A. Mullaney and R. L. Allemann, *Proteins: Struct. Funct. Genet.*, 2003, **51**, 216.
176. J. R. Schnell, H. J. Dyson and P. E. Wright, *Annu. Rev. Biophys. Biomol. Struct.*, 2004, **33**, 119.
177. R. S. Swanwick, P. J. Shrimpton and R. K. Allemann, *Biochemistry*, 2004, **43**, 4119.
178. R. P. Venkitakrishnan, E. Zaborowski, D. McElheny, S. J. Benkovic, H. J. Dyson and P. E. Wright, *Biochemistry*, 2004, **43**, 16046.
179. R. S. Sikorski, L. Wang, K. A. Markham, P. T. R. Rajagopalan, S. Benkovic and A. Kohen, *J. Am. Chem. Soc.*, 2004, **126**, 4778.
180. D. McElheny, J. R. Schnell, J. C. Lansing, H. J. Dyson and P. E. Wright, *Proc. Natl. Acad. Sci. USA*, 2005, **102**, 5032.
181. R. S. Swanwick, G. Maglia, L.-H. Tey and R. K. Allemann, *Biochem. J.*, 2006, **394**, 259.
182. L. Wang, S. Tharp, T. Selzer, S. J. Benkovic and A. Kohen, *Biochemistry*, 2006, **45**, 1383.
183. D. D. Boehr, H. J. Dyson and P. E. Wright, *Chem. Rev.*, 2006, **106**, 3055.
184. L. Wang, N. Goodey, S. J. Benkovic and A. Kohen, *Philos. Trans. Roy. Soc. B*, 2006, **361**, 1307.
185. R. K. Allemann, R. M. Evans, L.-H. Tey, G. Maglia, J. Pang, R. Rodriguez, P. J. Shrimpton and R. S. Swanwick, *Philos. Trans. Roy. Soc. B*, 2006, **361**, 1317.
186. L. Wang, N. M. Goodey, S. J. Benkovic and A. Kohen, *Proc. Natl. Acad. Sci. USA*, 2006, **103**, 15753.
187. D. D. Boehr, D. McElhenny, H. J. Dyson and P. E. Wright, *Science*, 2006, **313**, 1638.
188. P. L. Cummins, K. Ramnaryan, U. C. Singh and J. E. Gready, *J. Am. Chem. Soc.*, 1991, **113**, 8247.
189. P. L. Cummins and J. E. Gready, *J. Comp. Chem.*, 1998, **19**, 977.
190. R. Castillo, J. Andres and V. Moliner, *J. Am. Chem. Soc.*, 1999, **121**, 12140.
191. S. Hammes-Schiffer, *Biochemistry*, 2002, **41**, 13335.
192. P. K. Agarwal, S. R. Billeter and S. Hammes-Schiffer, *J. Phys. Chem. B*, 2002, **106**, 3283.

193. P. L. Cummins, S. P. Greatbanks, A. P. Rendall and J. E. Gready, *J. Phys. Chem. B*, 2002, **106**, 9934.
194. P. K. Agarwal, S. R. Billeter, P. T. R. Rajagopalan, S. J. Benkovic and S. Hammes-Schiffer, *Proc. Natl. Acad. Sci. USA*, 2002, **99**, 2794.
195. P. Shrimpton and R. K. Allemann, *Prot. Sci.*, 2002, **11**, 1442.
196. Y. Y. Sham, B. Ma, C.-J. Tsai and R. Nussinov, *Proteins: Struct. Funct. Genet.*, 2002, **46**, 308.
197. M. Garcia-Viloca, D. G. Truhlar and J. Gao, *Biochemistry*, 2003, **42**, 13558.
198. J. B. Watney, P. K. Agarwal and S. Hammes-Schiffer, *J. Am. Chem. Soc.*, 2003, **125**, 3745.
199. S. Ferrer, E. Silla, I. Tuñón, S. Marti and V. Moliner, *J. Phys. Chem. B*, 2003, **107**, 14036.
200. I. F. Thorpe and C. L. Brooks III, *J. Phys. Chem. B*, 2003, **107**, 14042.
201. S. Hammes-Schiffer, *Curr. Opinion Struct. Biol.*, 2004, **14**, 192.
202. K. F. Wong, J. B. Watney and S. Hammes-Schiffer, *J. Phys. Chem. B*, 2004, **108**, 12231.
203. I. F. Thorpe and C. L. Brooks III, *Proteins: Struct. Function Bioinf.*, 2004, **57**, 444.
204. I. F. Thorpe and C. L. Brooks III, *J. Am. Chem. Soc.*, 2005, **127**, 12997.
205. J. Pu, M. Garcia-Viloca, J. Gao, D. G. Truhlar and A. Kohen, *J. Am. Chem. Soc.*, 2005, **127**, 14879.
206. H. Alonso, M. B. Gilles, P. L. Cummins, A. A. Bliznyuk and J. E. Gready, *J. Comp.-Aided Molec. Des.*, 2005, **19**, 6807.
207. J. Pu, S. Ma, J. Gao and D. G. Truhlar, *J. Phys. Chem. B.*, 2005, **109**, 8551.
208. K. F. Wong, T. Selzer, S. J. Benkovic and S. Hammes-Schiffer, *Proc. Natl. Acad. Sci. USA*, 2005, **102**, 6807.
209. S. Hammes-Schiffer, *Acc. Chem. Res.*, 2006, **39**, 93.
210. J. Pang, J. Pu, J. Gao, D. G. Truhlar and R. K. Allemann, *J. Am. Chem. Soc.*, 2006, **128**, 8015.
211. A. Sergi, J. B. Watney, K. F. Wong and S. Hammes-Schiffer, *J. Phys. Chem. B*, 2006, **110**, 2435.
212. J. B. Watney and S. Hammes-Schiffer, *J. Phys. Chem. B*, 2006, **110**, 10130.
213. J. Pang and R. K. Allemann, *Phys. Chem. Chem. Phys.*, 2007, **9**, 711.
214. S. Hammes-Schiffer and J. B. Watney, *Philos. Trans. Roy. Soc. B*, 2006, **361**, 1365.
215. I. V. Khavrutskii, D. J. Price, J. Lee and C. L. Brooks III, *Prot. Sci.*, 2007, **16**, 1087.
216. P. L. Cummins, I. V. Rostov and J. E. Gready, *J. Chem. Theory and Comput.*, 2007, **3**, 1203.
217. C. A. Fierke, K. A. Johnson and S. J. Benkovic, *Biochemistry*, 1987, **26**, 4085.
218. A. Kohen and J. P. Klinman, *Chem. Biol.*, 1999, **6**, R191.
219. G. A. Veldink, *Biochemistry*, 1994, **33**, 3974.
220. M. H. Glickman, J. S. Wiseman and J. P. Klinman, *J. Am. Chem. Soc.*, 1994, **116**, 793.

221. M. H. Glickman and J. P. Klinman, *Biochemistry*, 1995, **34**, 14077.
222. N. Moiseyev, J. Rucker and M. H. Glickman, *J. Am. Chem. Soc.*, 1997, **119**, 3853.
223. K. W. Rickert and J. P. Klinman, *Biochemistry*, 1999, **38**, 12218.
224. A. M. Kuznetsov and J. Ulstrup, *Can. J. Chem.*, 1999, **77**, 1085.
225. V. B. O'Donnell, K. B. Taylor, S. Parthasarathy, H. Kühn, D. Koesling, A. Friebe, A. Bloodsworth, V. M. Darley-USmar and B. A. Freeman, *J. Biol. Chem.*, 1999, **274**, 20083.
226. E. I. Solomon, T. C. Brunold, M. I. Davis, J. N. Kemsley, S. K. Lee, N. Lehnert, F. Neese, A. J. Skulan, Y. S. Yang and J. Zhou, *Chem. Rev.*, 2000, **100**, 235.
227. M. J. Knapp and J. P. Klinman, *Eur. J. Biochem.*, 2002, **269**, 3113.
228. M. J. Knapp, K. Rickert and J. P. Klinman, *J. Am. Chem. Soc.*, 2002, **124**, 3865.
229. A. Kohen, *Prog. React. Kinet. Mech.*, 2003, **28**, 119.
230. V. C. Ruddat, S. Whitman, T.-R. Holman and C. F. Bernsconi, *Biochemistry*, 2003, **42**, 4172.
231. E. N. Segraves and T. R. Holman, *Biochemistry*, 2003, **42**, 5236.
232. M. J. Knapp and J. P. Klinman, *Biochemistry*, 2003, **42**, 11466.
233. Z. X. Liang and J. P. Klinman, *Curr. Opin. Struct. Biol.*, 2004, **14**, 648.
234. M. H. M. Olsson, P. E. M. Siegbahn and A. Warshel, *J. Am. Chem. Soc.*, 2004, **126**, 2820.
235. E. Hatcher, A. V. Soudackov and S. Hammes-Schiffer, *J. Am. Chem. Soc.*, 2004, **126**, 5763.
236. N. Lehnert and E. I. Solomon, *J. Biol. Inorg. Chem.*, 2003, **8**, 294.
237. M. H. M. Olsson, P. E. M. Siegbahn and A. Warshel, *J. Biol. Inorg. Chem.*, 2004, **9**, 96.
238. T. Borowski and E. Broclawik, *J. Phys. Chem. B*, 2003, **107**, 4639.
239. W. Siebrand and Z. Smedarchina, *J. Phys. Chem. B*, 2004, **108**, 4185.
240. I. Tejero, L. A. Eriksson, À. González-Lafont, J. Marquet and J. M. Lluch, *J. Phys. Chem. B*, 2004, **108**, 13831.
241. M. P. Meyer and J. P. Klinman, *Chem. Phys.*, 2005, **319**, 283.
242. I. Tejero, M. Garcia-Viloca, A. Gonzalez-Lafont, J. M. Lluch and D. M. York, *J. Phys. Chem. B.*, 2006, **110**, 24708.
243. E. Hatcher, A. V. Soudackov and S. Hammes-Schiffer, *J. Am. Chem. Soc.*, 2007, **129**, 187.
244. S. Chowdhury and R. Banerjee, *J. Am. Chem. Soc.*, 2000, **122**, 5417.
245. A. Dybala-Defratyka and P. Paneth, *J. Inorg. Biochem.*, 2001, **86**, 681.
246. R. Banerjee, D. G. Truhlar, A. Dybala-Defratyka and P. Paneth, in *Hydrogen Transfer Reactions*, ed. J. T. Hynes, J. P. Klinman, H.-H. Limbach and R. L. Schowen, Wiley, Weinheim, Germany, 2007, **Vol. 4**, pp. 1473–1495.
247. R. Banerjee, A. Dybala-Defratyka and P. Paneth, *Philos. Trans. R Soc. London B Biol. Sci.*, 2006, **361**, 1341.
248. A. Dybala-Defratyka, P. Paneth, R. Banerjee and D. G. Truhlar, *Proc. Natl. Acad. Sci. USA*, 2007, **104**, 10774.
249. J. A. Pople and R. K. Nesbet, *J. Chem. Phys.*, 1954, **22**, 571.

250. J. Pu, J. Gao and D. G. Truhlar, *Chem. Rev.*, 2006, **106**, 3140.
251. C. Alhambra, J. Gao, J. C. Corchado, J. Villà and D. G. Truhlar, *J. Am. Chem. Soc.*, 1999, **121**, 2253.
252. C. Alhambra, M. L. Sánchez, J. C. Corchado, J. Gao and D. G. Truhlar, *Chem. Phys. Lett.*, 2001, **347**, 512. Corrected version: 2002, **355**, 388.
253. M. Garcia-Viloca, C. Alhambra, D. G. Truhlar and J. Gao, *J. Am. Chem. Soc.*, 2002, **124**, 7268.
254. N. B. Colthup, L. H. Daly and S. E. Wiberley, *Introduction to Infrared and Raman Spectroscopy*, Academic Press, Boston, 1990, p. 177.
255. See, e.g., (a) ref. 228, (b) J. P. Klinman, *Pure Appl. Chem.*, 2003, **75**, 601 and (c) J. P. Klinman, *Philos. Trans. Roy. Soc. B*, 2006, **361**, 1323.
256. J. Basran, S. Patel, M. J. Sutcliffe and N. S. Scrutton, *J. Biol. Chem.*, 2001, **276**, 6234.
257. P. F. Faulder, G. Tresadern, K. K. Chohan, N. S. Scrutton, M. J. Sutcliffe, I. H. Hillier and N. A. Burton, *J. Am. Chem. Soc.*, 2001, **123**, 8604.
258. M. J. Sutcliff and N. S. Scrutton, *Eur. J. Biochem.*, 2002, **269**, 3096.
259. G. Tresadern, H. Wang, P. F. Faulder, N. A. Burton and I. H. Hillier, *Mol. Phys.*, 2003, **101**, 2775.
260. L. Masgrau, J. Basran, P. Hothi, M. J. Sutcliffe and N. S. Scrutton, *Arch. Biochem. Biophys.*, 2004, **428**, 41.
261. L. Masgrau, A. Roujeinikova, L. O. Johannissen, P. Hothi, J. Basran, K. E. Ranaghan, A. J. Mulholland, M. J. Sutcliffe, N. S. Scrutton and D. Leys, *Science*, 2006, **312**, 237.
262. M. J. Sutcliffe, L. Masgrau, A. Roujeinikova, L. O. Johannissen, P. Hothi, J. Basran, K. E. Ranaghan, A. J. Mulholland, D. Leys and N. S. Scrutton, *Philos. Trans. Roy. Soc. B*, 2006, **361**, 1375.
263. S. Nuñez, G. Tresadern, I. H. Hillier and N. A. Burton, *Philos. Trans. Roy. Soc. B*, 2006, **361**, 1387.
264. L. O. Johannissen, S. Hay, N. S. Scrutton and M. J. Sutcliffe, *J. Phys. Chem. B*, 2007, **111**, 2631.
265. K. E. Ranaghan, L. Masgrau, N. S. Scrutton, M. J. Sutcliffe and A. J. Mulholland, *ChemPhysChem*, 2007, **8**, 1816.
266. (a) Q. Cui and M. Karplus, *J. Am. Chem. Soc.*, 2002, **124**, 3093; (b) Q. Cui and M. Karplus, *J. Phys. Chem. B*, 2002, **106**, 7927; (c) Q. Cui and M. Karplus, *Adv. Protein Chem.*, 2003, **66**, 315.
267. B. C. Garrett, D. G. Truhlar, J. M. Bowman, A. F. Wagner, D. Robie, S. Arepalli, N. Presser and R. J. Gordon, *J. Am. Chem. Soc.*, 1986, **108**, 3515.
268. R. A. Marcus, *J. Chem. Phys.*, 1966, **45**, 2138.
269. D. C. Chatfield, R. S. Friedman, D. G. Truhlar, B. C. Garrett and D. W. Schwenke, *J. Am. Chem. Soc.*, 1991, **113**, 486.
270. W. H. Miller, *J. Chem. Phys.*, 1975, **62**, 1899.
271. D. C. Chatfield, R. S. Friedman, D. W. Schwenke and D. G. Truhlar, *J. Phys. Chem.*, 1992, **96**, 2414.
272. D. C. Chatfield, R. S. Friedman, G. C. Lynch, D. G. Truhlar and D. W. Schwenke, *J. Chem. Phys.*, 1993, **98**, 342.

273. J. Pu, J. C. Corchado and D. G. Truhlar, *J. Chem. Phys.*, 2001, **115**, 6266.
274. J. Pu and D. G. Truhlar, *J. Chem. Phys.*, 2002, **117**, 1479.
275. R. B. Bernstein, ed. *Atom-Molecule Collision Theory: A Guide for the Experimentalist*, Plenum, New York, 1979.
276. G. C. Schatz and A. Kuppermann, *J. Chem. Phys.*, 1976, **65**, 4642.
277. D. W. Schwenke, K. Haug, M. Zhao, D. G. Truhlar, Y. Sun, J. Z.-H. Zhang and D. J. Kouri, *J. Phys. Chem.*, 1988, **92**, 3202.
278. D. G. Truhlar, D. W. Schwenke and D. J. Kouri, *J. Phys. Chem.*, 1996, **94**, 7346.
279. R. E. Wyatt and J. Z. H. Zhang, ed. *Dynamics of Molecules and Chemical Reactions*, Marcel Dekker, New York, 1996.
280. A. Kuppermann and E. F. Greene, *J. Chem. Educ.*, 1968, **45**, 2361.
281. S. L. Mielke, K. A. Peterson, D. W. Schwenke, B. C. Garrett, D. G. Truhlar, J. V. Michael, M.-C. Su and J. W. Sutherland, *Phys. Rev. Lett.*, 2003, **91**, 63201.
282. T. Yamamoto, *J. Chem. Phys.*, 1960, **33**, 281.
283. W. H. Miller, S. D. Schwartz and J. W. Tromp, *J. Chem. Phys.*, 1983, **79**, 4889.
284. T. J. Park and J. C. Light, *J. Chem. Phys.*, 1989, **91**, 974.
285. P. N. Day and Donald G. Truhlar, *J. Chem. Phys.*, 1991, **94**, 2045.
286. F. Huarte-Larrañaga and U. Manthe, *J. Chem. Phys.*, 2001, **114**, 9683.
287. R. Zwanzig, *Annu. Rev. Phys. Chem.*, 1965, **16**, 67.
288. D. Chandler, *J. Chem. Phys.*, 1978, **68**, 2959.
289. J. T. Hynes, in *Theory of Chemical Reaction Rates*, ed. M. Baer, CRC Press, Boca Raton, FL, 1985, **Vol. 4**, pp. 171–234.
290. K. Haug, G. Wahnström and H. Metiu, *J. Chem. Phys.*, 1990, **92**, 2083.
291. E. Sim, G. Krilov and B. J. Berne, *J. Phys. Chem. A*, 2001, **105**, 2824.
292. I. R. Craig and D. E. Manolopoulos, *J. Chem. Phys.*, 2005, **123**, 34102.